iScience

CellPress
OPEN ACCESS

Article

Advancing coastal resilience: Coastal vulnerability assessment using cutting-edge space geodetic and optical imaging techniques

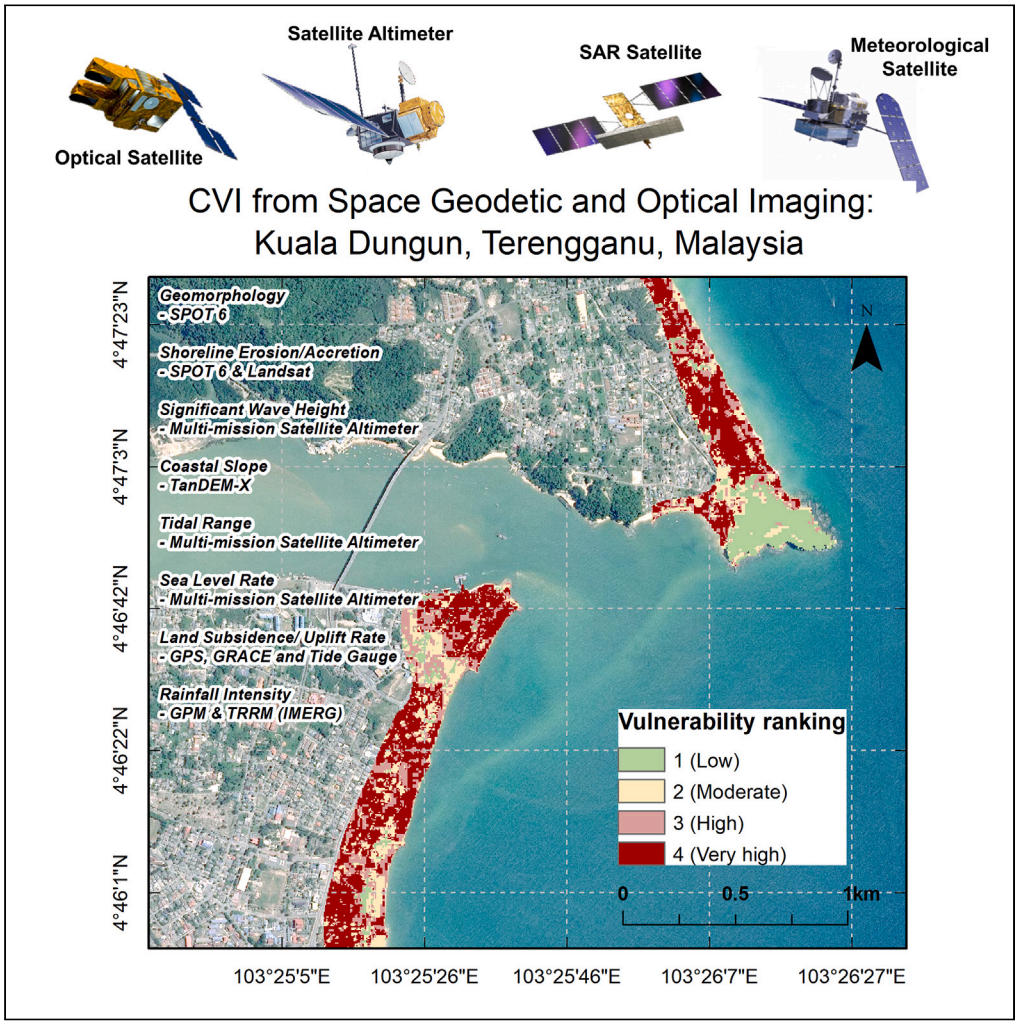

Amalina Izzati Abdul Hamid, Ami Hassan Md Din, Norhakim Yusof, Nazirah Mohammad Abdullah, Mohammad Hanif Hamden, Nur Adilla Zulkifli

amalina.izzati@utm.my (A.I.A.H.)
amihassan@utm.my (A.H.M.D.)

Highlights

Fully utilizing space technologies for Terengganu coastal vulnerability index

Spatiotemporal analysis for optimized conventional and new physical variables

The inclusion of eight parameters for CVI outperforms the conventional six parameters

Space technologies for coastal management proves to be both efficient and cost effective

Hamid et al., iScience 27, 110085
June 21, 2024
https://doi.org/10.1016/j.isci.2024.110085

iScience

CellPress
OPEN ACCESS

Article

Advancing coastal resilience: Coastal vulnerability assessment using cutting-edge space geodetic and optical imaging techniques

Amalina Izzati Abdul Hamid,[1,4,*] Ami Hassan Md Din,[1,*] Norhakim Yusof,[2] Nazirah Mohammad Abdullah,[3] Mohammad Hanif Hamden,[1] and Nur Adilla Zulkifli[1]

SUMMARY

Space geodetic and optical imaging techniques are employed to assess the coastal vulnerability index (CVI) in order to adapt to the contemporary approach to coastal classification. Satellite altimeter, Satellite Pour l'Observation de la Terre (SPOT) and integrated multi-satellite retrievals for GPM (IMERG) were among the satellite data used. The variables were deemed adequate based on the spatiotemporal estimates, then were quantified through expert-weighted scores and integrated into a single index over the Terengganu coastal area. The CVI findings performed better with eight variables, showing higher overall accuracy (70.83%), Kappa coefficient (59.02%), and area under curve (AUC) (0.8) than the conventional six variables. Vulnerability rankings are distributed relatively evenly across the Terengganu coast, with the moderate (2) ranking being the most predominant at 27.2% of the total area. Space geodetic and optical imagery techniques prove highly beneficial to CVI assessment, offering a viable alternative to traditional methods, especially for broader-scale coastal management.

INTRODUCTION

Coastal systems hold a substantial ecological and natural significance, and sustaining them is crucial because they provide essential ecosystem services for human well-being.[1,2] Due to their dynamic nature, coastal ecosystems are highly susceptible to environmental and anthropogenic pressures. Recent years have seen environmental dangers arising from unrestricted development and unsustainable use of coastal resources. Furthermore, the impact of climate change is increasingly pronounced on coastal areas, with the prevalence of rising sea levels in the years to come. The anticipated increase in global mean sea level (GMSL) is contingent on which the representative concentration pathway (RCP) emission scenario is followed, with a rise estimated to range between 0.43 m for RCP 2.6 and 0.84 m for RCP 8.5.[3] Nonetheless, irrespective of the pathway followed, the projected outcomes suggest unfavorable implications across various dimensions.

The notion of coastal vulnerability arises from interdisciplinary studies involving physical, ecological, and human characteristics that can alter coastal dynamics, gaining prominence as coastal areas globally confront heightened threats.[4,5] Due to the diversity in these factors, Earth scientists have undertaken investigations using multiple methods to categorize coastal areas by integrating these variables. They have developed several predictors, with one popular approach being the coastal vulnerability index or CVI. Over time, this approach gains favor due to its ability to acknowledge and select a number of prominent causes or variables to facilitate coastal classification in understandable information.[6] However, selecting from a number of crucial coastal variables to identify vulnerability proves to be very tricky. A study by Thieler and Hammar-Klose[7] addressing coastal vulnerability in the United States employed six accessible physical variables, namely geomorphology, shoreline erosion and accretion rates, coastal slope, rate of relative sea-level rise, tidal range, and mean wave height. Since then, scientists worldwide have regarded these variables as crucial for coastal assessments. Despite that, the varied geomorphological profiles of coastal regions globally should not be confined solely to the variables mentioned by Thieler and Hammar-Klose. Instead, the specific conditions of the research area must be taken into account. For instance, Pantusa et al.[8] introduced additional variables that characterize the study area, in addition to employing conventional variables to assess CVI.

Recently, space technologies have emerged as promising tools for large-scale mapping, propelled by revolutionary advancements in satellite techniques to extract reliable information.[9] In addition to capturing images and data across extensive geographical areas, space technologies are linked to cost-effectiveness for continuously monitoring and collecting data over time.[10] These technologies have also demonstrated the ability to monitor changes in timely updates, collect geospatial data in remote places, and rapidly acquire data. Therefore,

[1]Geospatial Imaging and Information Research Group (GI2RG), Faculty of Built Environment and Surveying, Universiti Teknologi Malaysia, Johor Bahru, Johor, Malaysia
[2]Geoinformation, Faculty of Built Environment and Surveying, Universiti Teknologi Malaysia, Johor Bahru, Johor, Malaysia
[3]Department of Technology and Natural Resources, Faculty of Applied Sciences and Technology, Universiti Tun Hussein Onn Malaysia, Parit Raja, Johor, Malaysia
[4]Lead contact
*Correspondence: amalina.izzati@utm.my (A.I.A.H.), amihassan@utm.my (A.H.M.D.)
https://doi.org/10.1016/j.isci.2024.110085

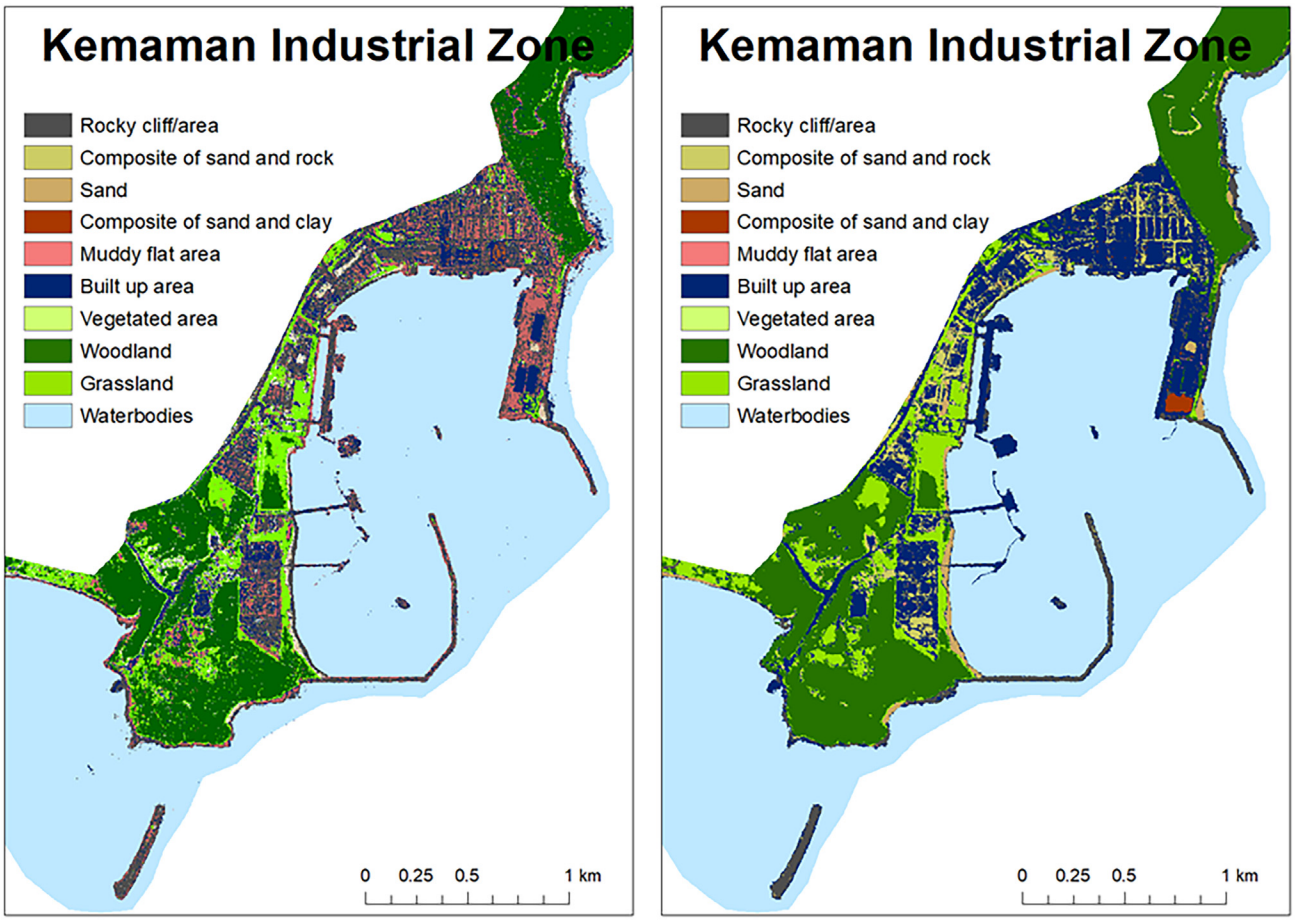

Figure 1. Comparison of different classification techniques at Kemaman industrial zone
(left) derived from supervised classification and (right) is from SegOptim.

by fully adopting these technologies, this paper presents a method using space-geodetic satellites and optical imaging techniques to derive coastal variables required for assessing CVI. Despite these advancements, space technologies are still lacking in terms of optimal satellite sensor and data fusion strategies. For this reason, the derived variables in this paper were subjected to a spatiotemporal analysis to optimize their utilization, ensuring that CVI runs on clean, accurate, and meaningful data.

RESULTS AND DISCUSSIONS

This section delves into the findings and their analyses, beginning with the spatiotemporal analysis for each physical variable, then comparing the derived CVI from the weighted variables, and concluding with an evaluation of the final CVI.

Spatiotemporal analysis of physical variable

Regional-scale CVI becomes feasible with the advent of space-based measurements that offer widespread information on landscapes and oceans. In this paper, a spatiotemporal analysis of each physical variable was performed in order to maximize the information extracted by cutting-edge space geodetic and optical imagery. The following findings based on each physical variable culminate in the formulation of CVI.

Geomorphology

Considering the large landscape image involved, different image classification techniques can present a certain rebuttal on which classification is reliable. A comparison was conducted between supervised and segmented object-based segment analysis (OBIA), utilizing 27 coastal global navigation satellite system (GNSS) control points and focusing on overall accuracy (*OA*) and Cohen's *Kappa*. This analysis concentrated on specific sites representing diverse environmental conditions, with Figure 1 depicting the disparities between the two classifications at the Kemaman industrial zone in Terengganu.

It is evident from Figure 1 that supervised classification tends to exaggerate the composition of land cover, notably misclassifying the majority of built-up areas as muddy flat areas. In contrast, SegOptim exhibits immaculate classification, accurately categorizing features based on

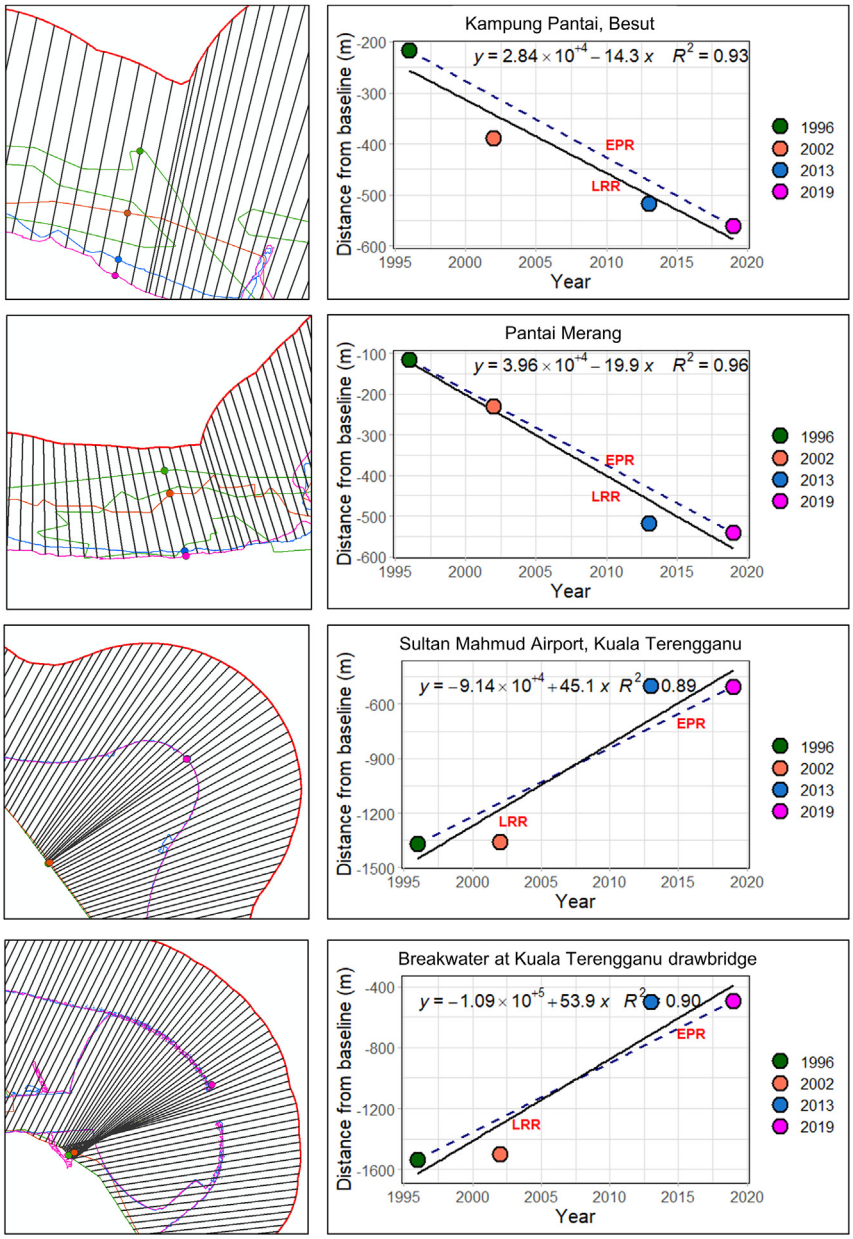

Figure 2. Terengganu shoreline's multi-temporal position and its linear regression

The shoreline's multi-temporal position and its linear regression at (A) Kampung Pantai, Besut (B) Pantai Merang, (C) Sultan Mahmud Airport, Kuala Terengganu, and (D) Breakwater at Kuala Terengganu drawbridge.

the given training samples. Among all classes, compositional characteristics of sand, built-up area, and grassland show refinement in producer's accuracy, whereas features on composites of sands and clays as well as built-up area exhibit a slight refinement in user's accuracy when segmented OBIA is used. The combined supervised with segmented OBIA yields and *OA* of a score of 71.43%, higher than the score generated from the supervised classification alone, which is 42.86%. *Kappa* metric also improves significantly when segmented OBIA is incorporated, showing a substantial increase of around 23%.

Shoreline erosion or accretion

The rate-of-change extracted from four temporal shoreline positions was spatially quantified over the transects using the linear regression rate (LRR) analytic approach. This type of analytical is chosen for CVI assessment as it incorporates all shorelines involved in the computation,

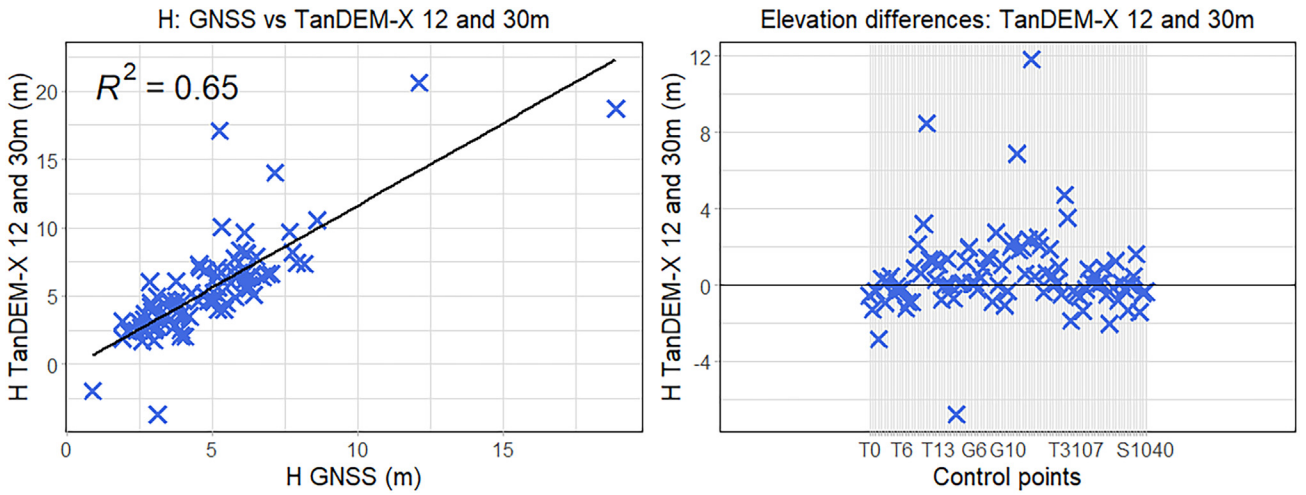

Figure 3. The correlation and elevation difference of H from TanDEM-X and GSS points

resulting in robust performance across a wide range of distributions.[11,12] Figure 2 depicts the notable erosion/accretion and its rate-of-change based on LRR estimates. This table also included the end-point-rate (*EPR*) analytical, comparing these two approaches.

Significant retreat is observed at E1 and E2, while E3 and E4 experience accretion. Based on the LRR analytic rate estimates, Terengganu's shoreline undergoes average erosion and accretional rates of −1.72 m/yr and 3.56 m/yr, respectively. The transects contributing to erosion are 63.56%, indicating that the majority of the Terengganu coast is eroding at alarming rates. Kampung Pantai, Besut (E1), as shown in Figure 2, experiences a substantial retreat of −14.3 m/yr, attributed to the coastal land loss events that potentially occurred after 2002.

Coastal slope

For the spatiotemporal analysis of the coastal slope in Terengganu, 98 GNSS control points were employed, and their orthometric heights (*H*) were calculated. These data were then compared with TanDEM-X in terms of mean bias (*MB*), root-mean-square error (*RMSE*), and correlation. The statistical analysis reveals a correlation of 0.65 for TanDEM-X with 12 m combined 30 m resolutions. As shown in Figure 3, the elevation difference of H from GNSS and TanDEM-X also shows a good correlation with TanDEM-X points relative to the zero value. In summary, in addition to satisfactory correlation metric, TanDEM-X with combined 12 m and 30 m resolutions exhibits lower *RMSE* (2.42 m) and *MB* (0.562 m) metrics, rendering it adequate for the CVI assessment of coastal slope.

Significant wave height

Significant wave height from satellite altimeters and coastal and offshore buoys in the South China Sea were retrieved for spatiotemporal analysis, emphasizing time series pattern, correlation, and statistical analyses. Figure 4 demonstrates that among the four buoys utilized, the Sarawak buoy shows a strong agreement in linear correlation analysis with altimetric significant wave height. The correlation metric at Sarawak buoy yields a confidence result of 0.941, with an estimated *RMSE* of 0.165 m.

Nevertheless, the significant wave heights observed from the SOTONG and AWAC buoys clearly show a noticeable disparity when compared to altimetry data, yet still marginally align with the buoy pattern. The diminished correlation metrics at both buoys are attributed to a lack of data, which may reduce the precision. Meanwhile, the buoy located in the Sabah region's sea demonstrates a substantial correlation between altimetric and buoy-derived significant wave heights, as proven by the correlation and *RMSE* values of 0.931 and 0.168 m, respectively. Table 1 shows that the statistical analysis of significant wave height from both measurements reveals satisfactory scores that are acceptable for use in the CVI assessment.

Tidal range

To establish the optimal mean tidal range for use in CVI assessment, the tidal range derived from the integrated UTM20[13] and altimeter missions were assessed with mean tidal range data from 11 Peninsular Malaysia tide gauge stations. Figure 5 depicts the correlation and line patterns of tidal ranges, indicating a robust agreement between UTM20 and the observed mean tidal range from tide gauges, in comparison to the linear correlation between altimeter-derived tidal range and mean tidal range from tide gauges.

This is further substantiated by the near-optimal coefficients of 0.994 and *RMSE* of 0.164 m, showcasing a difference of around 0.6 m when compared to *RMSE* of the altimetric-derived tidal range, as presented in Table 2. Despite the need for significant enhancements in satellite altimeter-derived tidal range, the current viable solution to enhance the satellite altimeter-derived tidal model involves integrating it with conventional tide gauge-derived tidal information. This integrated approach is deemed sufficient for assessing tidal range through space

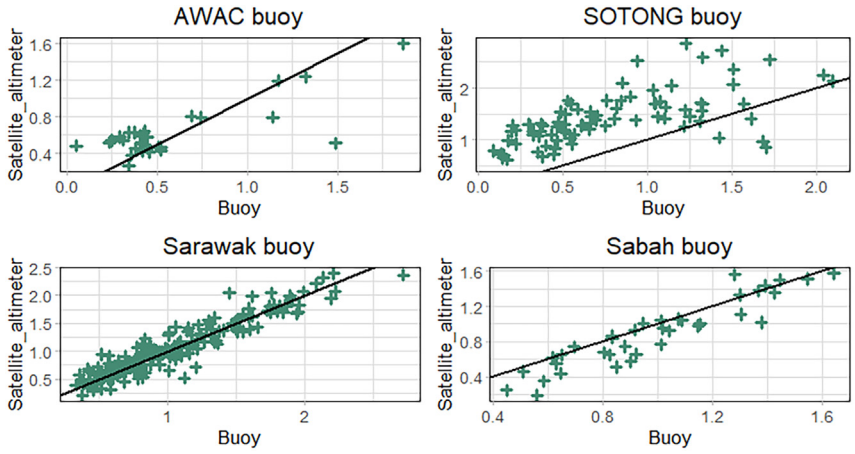

Figure 4. Time series and correlation analyses between altimetric and buoy significant wave heights
Units are in meters.

measurements. Based on this analysis, it is reasonable to assert that the UTM20 model outperforms the tidal range from the satellite altimeter and is thus suitable for CVI assessment.

Sea level rate

Sea level rate is a time series analysis, and information on the signal frequency domain is not as crucial as tide analysis. Hence, sea level anatomy (SLA) data, crucial for rate computation, were examined from both tide gauge and altimetric datasets in five east coast stations of Peninsular Malaysia. The time series plots of altimetric and tidal records at all tide gauge stations exhibit similar patterns and linear correlation, indicating good agreement across all stations. Figure 6 shows the linear correlation observed at the East Coast tide gauge stations. The correlation analysis resulted in an average of 92% confidence level for all stations, with correlation values ranging from 0.89 to 0.94. Moreover, all altimetry data achieved *RMSE* between 0.04 m and 0.05m, respectively, yielding a near-optimal value of 0, thus appropriate for the CVI assessment.

Land subsidence or uplift rate

Since the sea level data in this study did not incorporate land subsidence/uplift from tidal data, a separate land subsidence/uplift model was included. Figure 7 demonstrates the land subsidence/uplift rate over the Terengganu region as calculated by Zulkifli.[14] These rates were determined from year 1999–2017 by assimilating multi-sensor geodetic techniques to enhance land subsidence/uplift estimates. In Figure 7, the dark blue color signifies a land uplift, which is apparent in urban areas of Kuala Terengganu, Al-Muktafi Billah Shah town, Dungun, and Chukai. While seismic activities can induce land uplift, it can also be attributed to various factors, as in the case of coastal uplift in Kuala Terengganu, which is most likely the result of aggressive coastal protection and nourishment practices due to mitigating severe erosion. Nonetheless, notable land subsidence at Marang coasts, as shown in Figure 7, is a result of substantial alterations in general, in terms of sediment transport, wave, monsoon, wind, tidal inundation, and urban expansion.[15]

Rainfall intensity

Based on the annual accumulated rainfall data obtained, the IMERG product is tested in terms of pattern and correlation against 14 rain gauges dispersed across southern Terengganu. The rain gauge data were collected from 2000 to 2016. Figure 8 shows the annual precipitation pattern from IMERG is underestimated compared to the precipitation recorded by rain gauges. Nevertheless. It closely resembles the

Table 1. Mean difference, RMSE, and R^2 value for significant wave height data

Station	Mean Bias (m)	RMSE (m)	R^2
Significant wave height			
AWAC	0.046	0.261	0.784
SOTONG	0.634	0.758	0.633
Sarawak	0.011	0.165	0.941
Sabah	−0.094	0.168	0.931
Average	0.261	0.338	0.784

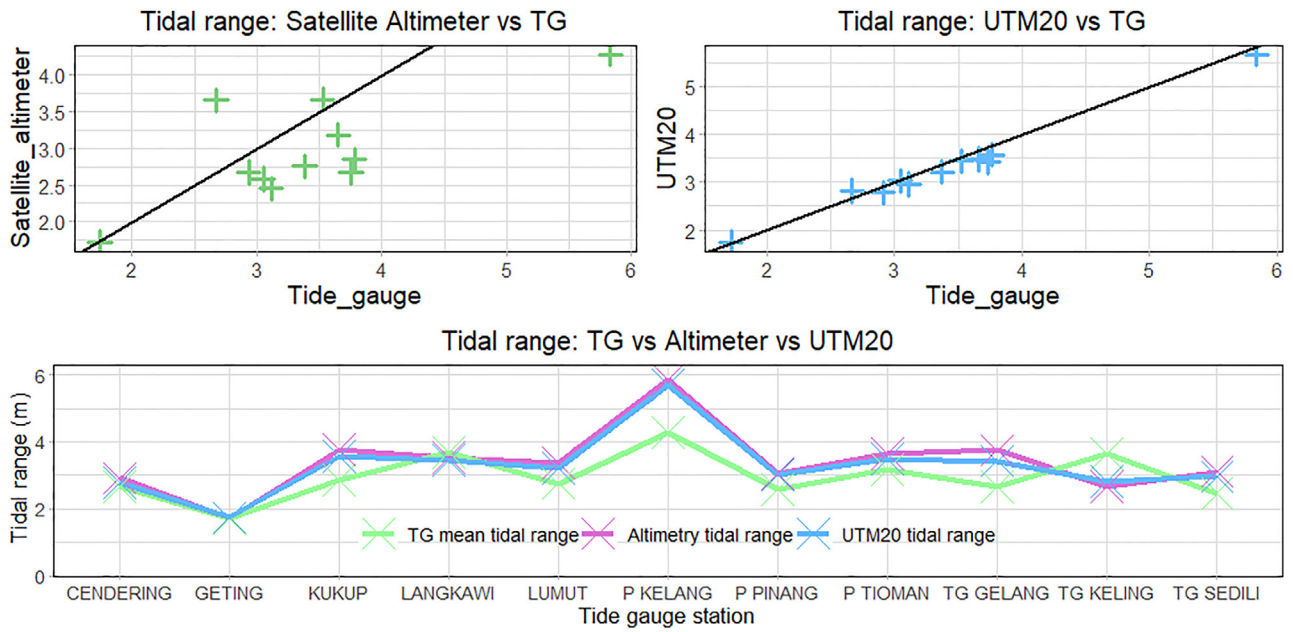

Figure 5. Tidal range correlation analysis and line pattern
Units are in meters.

precipitation pattern observed in rain gauge data. According to Mahmud et al.,[16] satellite-derived precipitation tends to underestimate heavy rainfall in stations located in East Malaysia, thus lending credence to the IMERG's underestimated precipitation readings of this study.

Notwithstanding, the average *RMSE* and R^2 metrics shown in Table 3 are 8.32 mm and 0.64, respectively. These results indicate a satisfactory performance of IMERG in assessing annual spatial rainfall variability in Malaysia's tropical humid equatorial region. Furthermore, the detection accuracy of precipitation events in the IMERG product was assessed using metrics such as probability detection (*POD*), false alarm ratio (*FAR*), and crucial success index (*CSI*). The ideal *POD* and *CSI* values are 1, while *FAR* is 0. The overall *POD* is 0.94, with SK Kijal having the highest *POD* value of 0.97 and Tebak station exhibiting the lowest *POD* of 0.92. However, the *FAR* score for SK Kijal is 0.56, the highest among other stations, indicating around 56% of the expected precipitation but no rainfall from rain gauges. The average *FAR* is 0.479, with the Jengai station registering the lowest score of 0.376. Generally, the *CSI* for all precipitation products ranges from 0.432 to 0.6, suggesting that around half of the precipitations are correctly assessed.

Comparison between six and eight parameters of CVI

The final parameters in Table 4, are summarized from the contribution of each variable to the final estimated vulnerability score derived from space-based information on physical variables. Each parameter has a relative vulnerability score given to it, ranging from 1 to 5, with 1 denoting very low vulnerability while 5 denoting very high vulnerability.

Three of the seven experts' weightings were disregarded as their consistency ratio exceeded the 0.1 threshold. The final weights were computed to three decimal places to improve the visibility of differences between variables.[17] Overall, the Terengganu coast vulnerability is predominantly influenced by shoreline erosion, which holds the highest overall weight of 0.316, followed by significant wave height (0.178), sea level rate (0.129), geomorphology (0.09), mean tidal range (0.085), coastal slope (0.067), and land subsidence (0.045), while rainfall intensity carries the lowest weight at 0.021.

The final CVI was calculated, and the assigned vulnerability categories (low, moderate, high, and very high) were determined and compared to 24 CVI control points derived from extensive GNSS and site surveys. This comparison involved evaluating *OA*, *Kappa* metric, receiver operating characteristic (ROC) curve and area under curve (AUC), to ascertain whether the vulnerability assessment of the Terengganu coast is better suited with six or eight parameters of CVI. Major refinement of producer's and user's accuracies from six to eight

Table 2. Mean difference, RMSE, and R^2 values for tidal range estimates

Model	Mean Bias (m)	RMSE (m)	R^2
Mean tidal range			
Satellite altimeter	−0.447	0.783	0.740
UTM20	−0.115	0.164	0.994

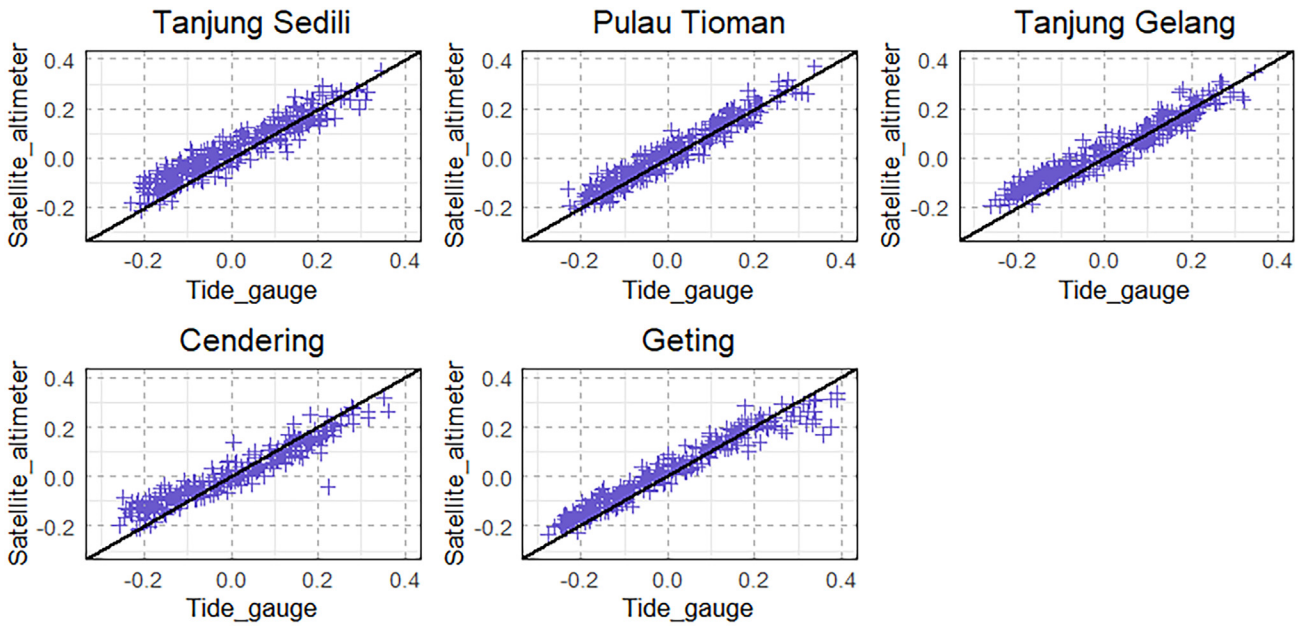

Figure 6. Time series and correlation analysis between altimetric and tidal SLA in Cendering tide gauge station in Terengganu
Units are in meters.

parameters, with a substantial increase in both accuracies of vulnerability categories of moderate, high, and very high was determined. The very high (4) ranking indicates an increase in the producer's accuracy from 50% to 75% between six and eight parameters but decreases from 66.67% (six parameters) to 54.55% (eight parameters), implying that at least 20% is incorrectly classified between both accuracies of eight parameters.

The eight parameters of CVI results in an *OA* of 70.83% and a *Kappa* metric of 59.02%. The scores for eight parameters substantially surpass the accuracy scores of six parameters, which are 45.8% for *OA* and 26.06% for the *Kappa* score, reflecting a 32% improvement in accuracy. Figure 9 depicts the ROC curve and *AUC* metrics for six and eight parameters, with eight parameters transcending the six. As the developed CVI revolves around the multi-class problem, the heuristic approach was utilized to break the multi-class classification problem into multiple binary classifications, allowing for the training of individual models for each case. The ROC curves represent the performance of four

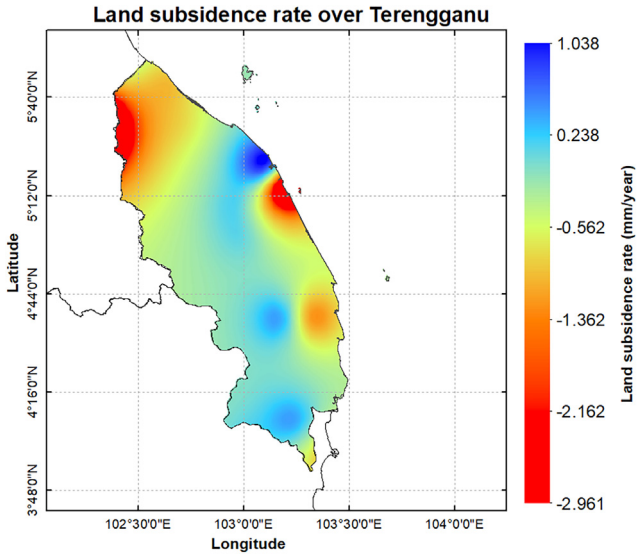

Figure 7. Land subsidence/uplift rate over the Terengganu region

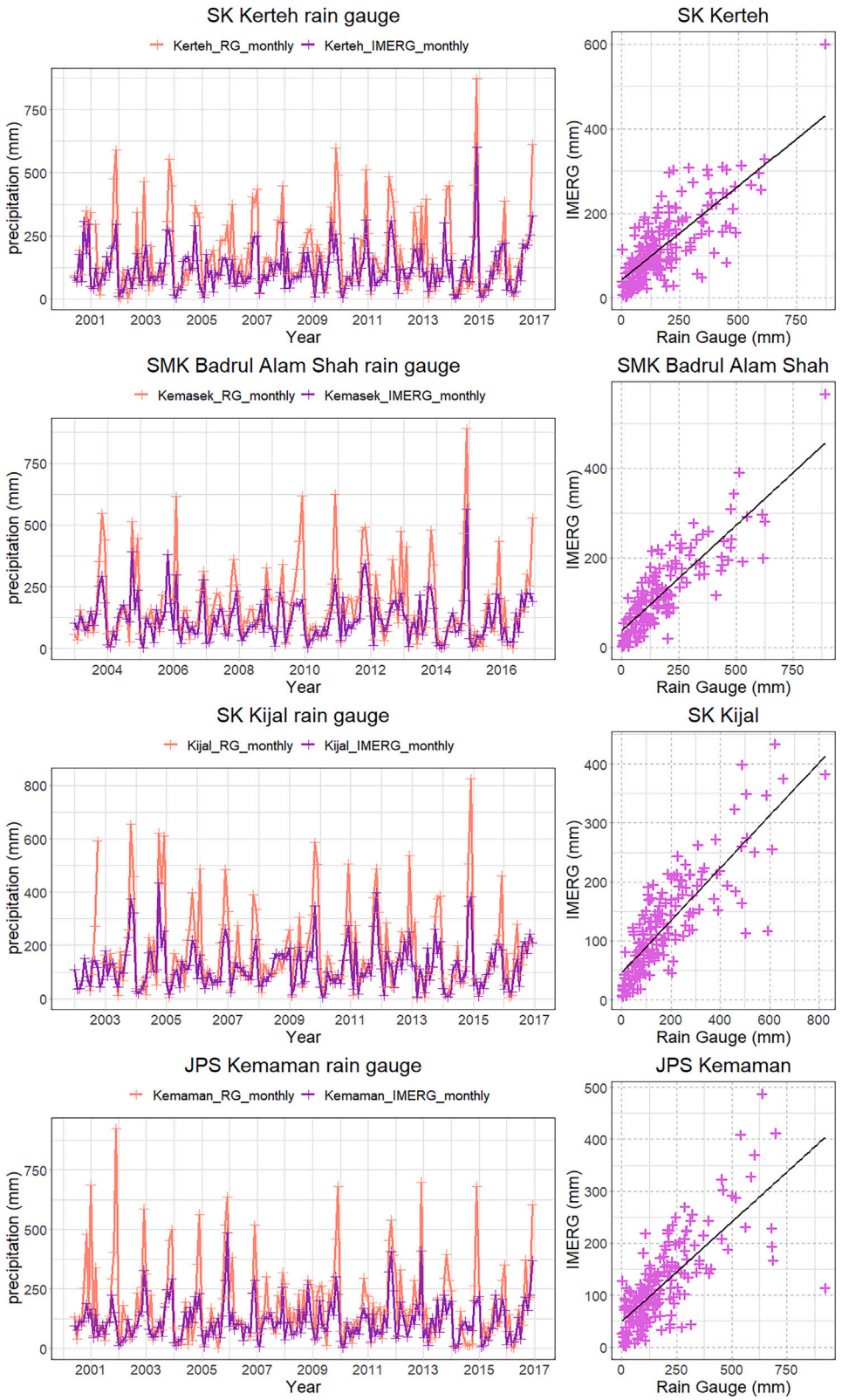

Figure 8. Terengganu coastal rain gauge stations pattern and correlation plot

Table 3. Evaluation metrics between IMERG and rain gauge precipitation data

Station	Mean bias (mm)	RMSE (mm)	R^2	POD	FAR	CSI
Jengai	−1.0386	9.8696	0.5763	0.94	0.3757	0.6004
Billah	0.1044	9.0506	0.6140	0.9694	0.4828	0.5089
Pasir Raja	0.0261	8.8283	0.6011	0.9491	0.4041	0.5775
SK Kerteh*	0.8826	8.170	0.6285	0.9251	0.4929	0.4871
SMK Badrul*	0.6722	7.8441	0.6364	0.9284	0.5135	0.4689
Tebak	0.1135	8.7741	0.6237	0.9217	0.4411	0.5335
Seri Bandi	0.0675	8.35	0.6968	0.9332	0.47	0.5107
Kg. Ibok	0.4336	8.0388	0.7156	0.9475	0.5108	0.4762
SK Kijal*	1.1762	7.7478	0.6881	0.9698	0.5616	0.4325
Air Putih	0.7019	7.6163	0.5708	0.9294	0.4739	0.5058
SK Pasir Gajah	0.3854	7.9461	0.7353	0.9231	0.4577	0.5189
JPS Kemaman*	0.611	7.5745	0.7009	0.9418	0.5167	0.4693
Kg. Ban Ho	0.1883	8.4111	0.5637	0.9512	0.4832	0.5034
Hulu Jabor	0.5396	8.2942	0.6605	0.9444	0.5282	0.4590
Average	**0.3474**	**8.3225**	**0.6437**	**0.941**	**0.4794**	**0.5037**

*Terengganu coastal rain gauge stations; *SK, Sekolah Kebangsaan (primary school).
*SMK, Sekolah Menengah Kebangsaan (secondary school); *Kg., Kampung (village).
*JPS, Malaysian Department of Irrigation and Drainage.

vulnerability categories. The eight parameters of CVI exhibit an excellent classifier, evident by lines closer to the axes, except the Low_VeryHigh category, which is closer to the gray line and suggests a less effective classifier. The corresponding *AUC* metrics in eight parameters exceed 0.8 across tested categories, except for the Low_VeryHigh category. This indicates a more than 80% prediction accuracy for the tested model. In conclusion, the metrics calculated from the confusion matrix and ROC curve demonstrate that the CVI generated from eight parameters presents a convincing outcome, outperforming the six parameters.

Terengganu CVI assessment from physical variables

The ranking of physical variables ranking was assessed. Sandy coastline and woodland classes constitute the majority of geomorphological features. The area surrounding Pantai Batu Buruk, Kuala Terengganu, Teluk Bidara, and Kuala Dungun is dominant in terms of very high-ranking (5) scores. Based on the computed area of Terengganu geomorphology, the classification predominantly falls into the low (1) category with a score of 47.5%, largely found in woodland areas, and high (4) score with a percentage of 18.9%, which is mostly observed in coastal areas.

Terengganu coastal areas exhibit around 83.9% high (4) vulnerability ranking, with 11.01% indicating moderate (3) erosion. According to rate estimated from LRR, the average rate of changes in Terengganu coast is 0.24 m/yr with average erosion and accretional rates are −1.72 m/yr and 3.65 m/yr, respectively. Mountainous areas exhibit a low (1) vulnerability score, whereas slopes in urban and industrial areas

Table 4. Final CVI ranking based on eight physical variables

	Ranking of coastal vulnerability index				
	Very low	Low	Moderate	High	Very High
VARIABLE	1	2	3	4	5
Geomorphology	Rocky cliff/area	Composites of sands and rocks	Sands	Composites of sands and clays	Muddy flat area
Shoreline erosion (m $year^{-1}$)	36.07–53.24	18.90–36.06	1.73–18.89	−15.44–1.72	−15.45–−32.62
Sea level rate (mm yr^{-1})	2.75–3.32	3.33–3.89	3.90–4.47	4.48–5.04	5.05–5.61
Mean tidal range (m)	4.89–5.91	3.87–4.88	2.85–3.86	1.83–2.84	0.80–1.82
Significant wave height (m)	0.22–0.56	0.57–0.90	0.91–1.23	1.24–1.56	1.57–1.90
Coastal slope (%)	>15.10	10.10–15.00	5.10–10.00	2.10–5.00	<2.00
Land subsidence (mm $year^{-1}$)	0.24–1.04	−0.55 – 0.23	−1.35–−0.56	−2.15–−1.36	−2.96–−2.16
Rainfall intensity (mm $hour^{-1}$)	<0.30	0.31–0.33	0.34–0.36	0.37–0.39	>0.40

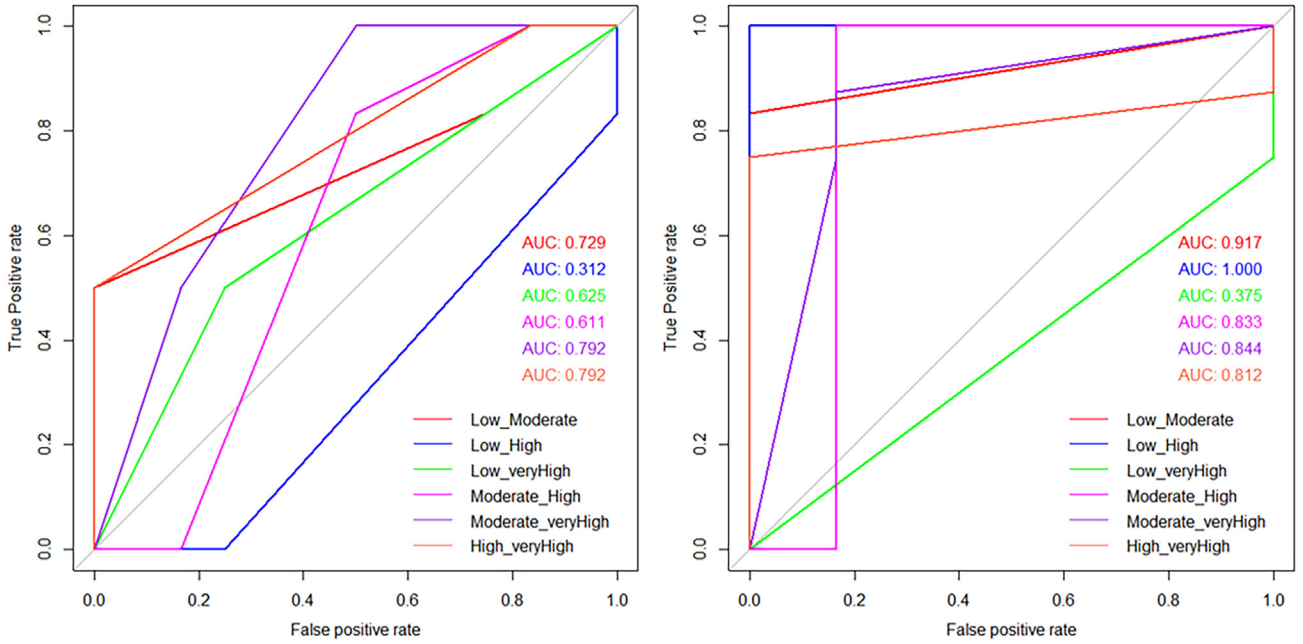

Figure 9. ROC curves and AUC metrics for six parameters (left) and eight parameters (right)

attain the highest score of very high (4) ranking, constituting 12% of the overall ranking. According to the land subsidence/uplift rates, 43.8% of Terengganu coasts have moderate (3) subsidence ranging from −1.35 mm/yr to −0.56 mm/yr, with the Marang coast having the highest ranking. In addition, the rainfall intensity over the Terengganu coast, estimated from IMERG data for the period of 2000–2019, has high (4) ranking in the most northern part of the Terengganu coast and moderate (3) ranking in the rest of Terengganu coast. Figure 10 displays the vulnerability ranking assigned to shoreline erosion, coastal slope, land subsidence/uplift rate, and rainfall intensity across the Terengganu coast.

The seasonal circulation significantly influences the variability of waves northeast of the South China Sea[18] and intensifies larger waves. This results in the central part of the South China Sea near the Terengganu coasts being moderately (3) exposed to coastal risk, while the northern and southern parts are categorized as low (2) in vulnerability. Meanwhile, in this study, areas with low tidal ranges are classified as highly vulnerable since micro tidal areas are more prone to increased storm risk since they are always "near" high tide. The tidal range along the Terengganu coast has been classified as high (4) risk in the northern part and moderate (3) risk in the most southern part. After assigning the risk value of the sea level rate, the dominated ranking is identified, with the low (2) ranking predominating over the Terengganu coast. The final vulnerability ranking of significant wave height, tidal range, and sea level rate are shown in Figure 11.

The final CVI were categorically assigned based on the 25th, 50th, and 75th percentiles, based on Thieler and Hammar-Klose's study.[7] Figures 12, 13, 14, and 15 show the final CVI derived from eight parameters mapped along the Terengganu coast. The vast expanse of the Terengganu coast is part of a broad alluvial plain, with sandy beaches stretching nearly the entire length of the coast. As a result, the highest vulnerability to rising sea levels is mostly found in low-lying areas with mudflats, composites of sands and clays, or sands only. The highest scores are observed in Pantai Penarik and Pantai Rusila at Kuala Terengganu, Pantai Merchang at Marang, Pantai Teluk Bidara Pantai Teluk Lipat at Kuala Dungun, and Pantai Paka. The most affected areas are mostly identified in urban and residential areas near the coasts, with a high (3) risk to very high (4) ranking. The residential areas at Pantai Penarik, Pantai Rusila, Pantai Teluk Lipat, and Pantai Paka are known for their erosive trend, prompting active restoration works in these areas over the years.

Contrary to expectations, the CVI based on eight parameters reveals that the urban areas of Kuala Terengganu, particularly those near the Sultan Mahmud Airport, have a high (3) to moderate (2) vulnerability ranking. Despite being known as coastal area with a high risk of severe erosion due to tarmac extension, the situation is still under control and deemed safer compared to other coastal areas with high-ranking coastal areas. This is probably because stakeholders are aggressively restoring Kuala Terengganu urban areas by constructing rip rap and compacting sand on the beach for maintenance purposes.[19] Low (1) vulnerability areas, defined by scores less than 1.45, can be found in the majority of high-lying woodlands, such as Rimba Bandar Bukit Bauk, Dungun, and Bukit Kambing, Kijal. Additionally, sandy beaches undisturbed by development, including Pantai Mengabang Panjang and Pantai Mengabang Lekar in Kuala Terengganu, and the pine forest around the coastal area in Sungai Paluh, Kerteh are also classified in low (1) vulnerability ranking.

Following that, the census parameter of the population in the Terengganu region is incorporated for further analysis of CVI. Figure 16 depicts the municipal population exposed due to CVI, with a very high (4) ranking dominating the population exposed by 35.7%. The highest at-risk population is concentrated in densely populated areas, well-known for their pronounced erosion, where the distance to the seafront is close to zero. Around 1,300 people are exposed to the municipal area of Rusila, and 1,200 people are exposed to Teluk Lipat, which has very

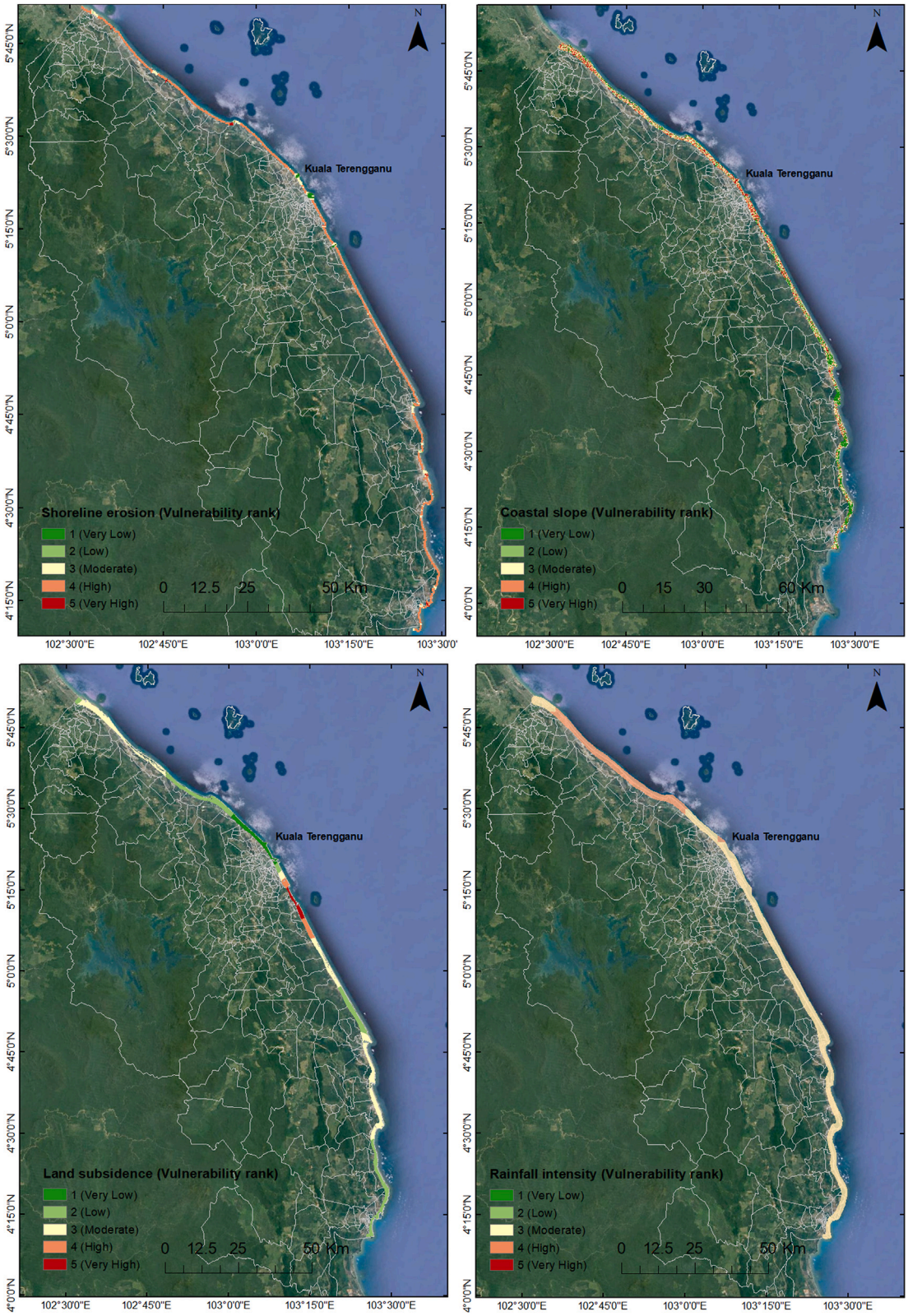

Figure 10. Vulnerability ranking of shoreline erosion, coastal slope, land subsidence/uplift rate, and rainfall intensity over Terengganu

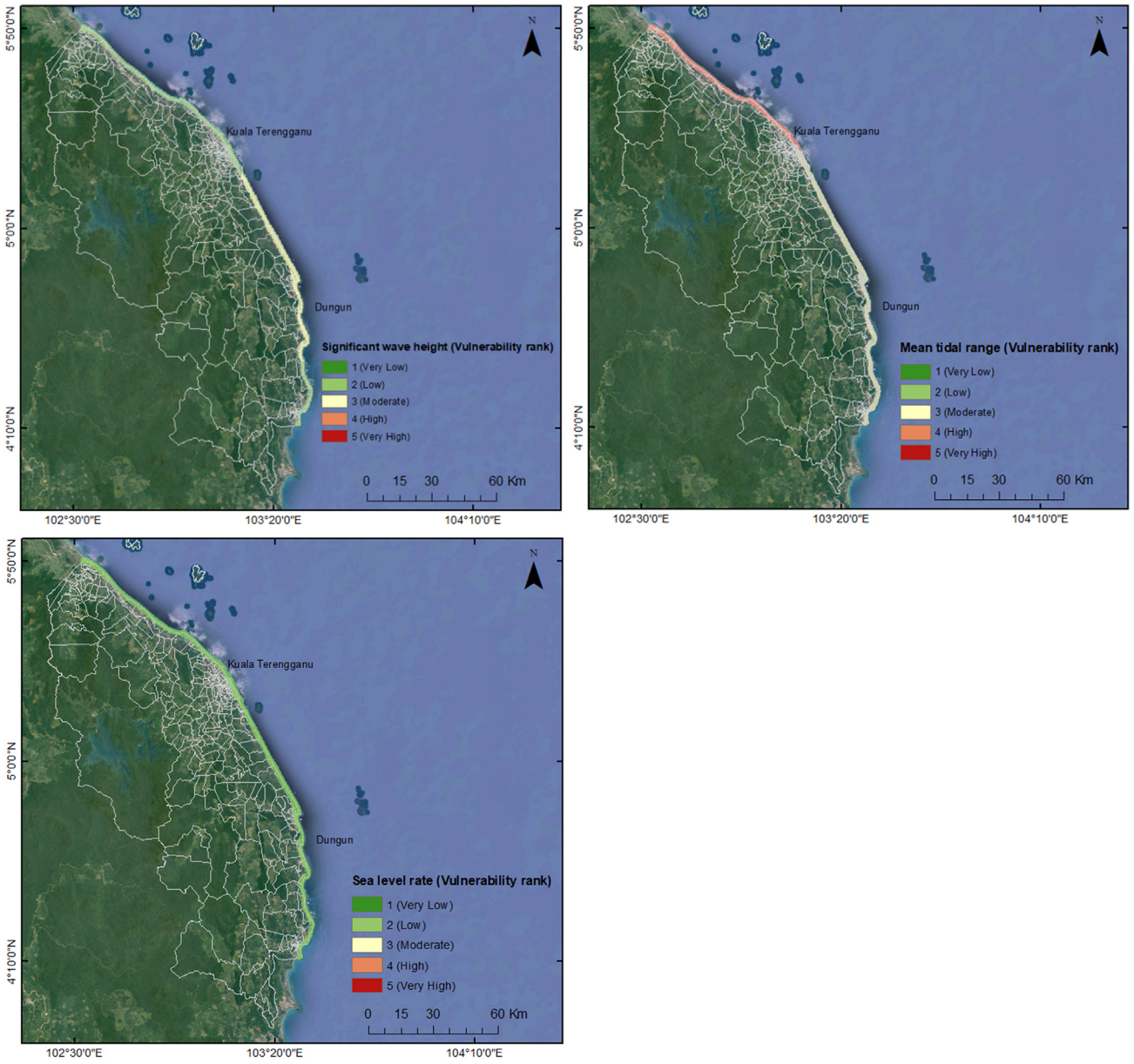

Figure 11. Vulnerability ranking of significant wave height, tidal range, and sea level rate over Terengganu

high vulnerability scores. According to CVI, other areas with substantial population exposure include the Geliga municipal area, encompassing around 900 population, surrounded by Sungai Marang and close to the Kemaman industrial zone. The residential area of Fikri in Chukai, with a population of around 1,000 people, is densely populated and is also expected to experience severe erosion. In brief, with a few exceptions, CVI correctly designated coastal areas subjected to continuous erosion.

Conclusion

This study has explicitly examined the impact of coastal changes based on physical variables from advanced space-geodetic and optical techniques, focusing specifically on the coastal areas of Terengganu (see Figure 17). The CVI was predicated on the physical variables and was rationally selected according to their importance on the study area. The additional physical variables for the CVI assessment, which were land subsidence and rainfall intensity, had been incorporated along with the conventional six physical variables of geomorphology, shoreline erosion, and coastal slope, significant wave height, tidal range, and sea level rate The data selected were specifically tailored to the study area. Following the spatiotemporal analysis of the space-based physical variables, weighted scores based on several correspondents were assigned to all eight physical variables, representing a level of relevance to determine the final vulnerability levels.

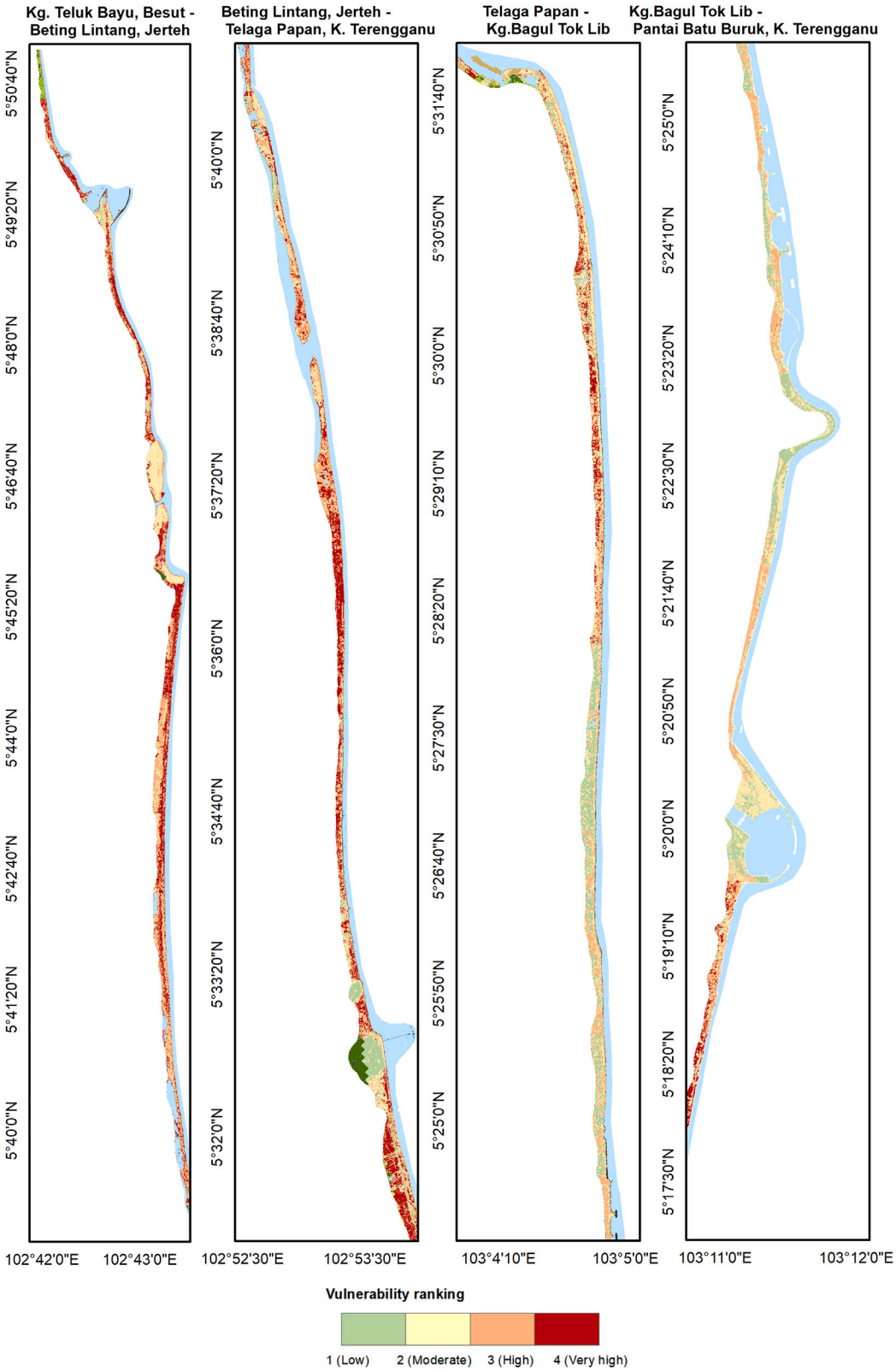

Figure 12. Final CVI from eight parameters from Jerteh to Kuala Terengganu

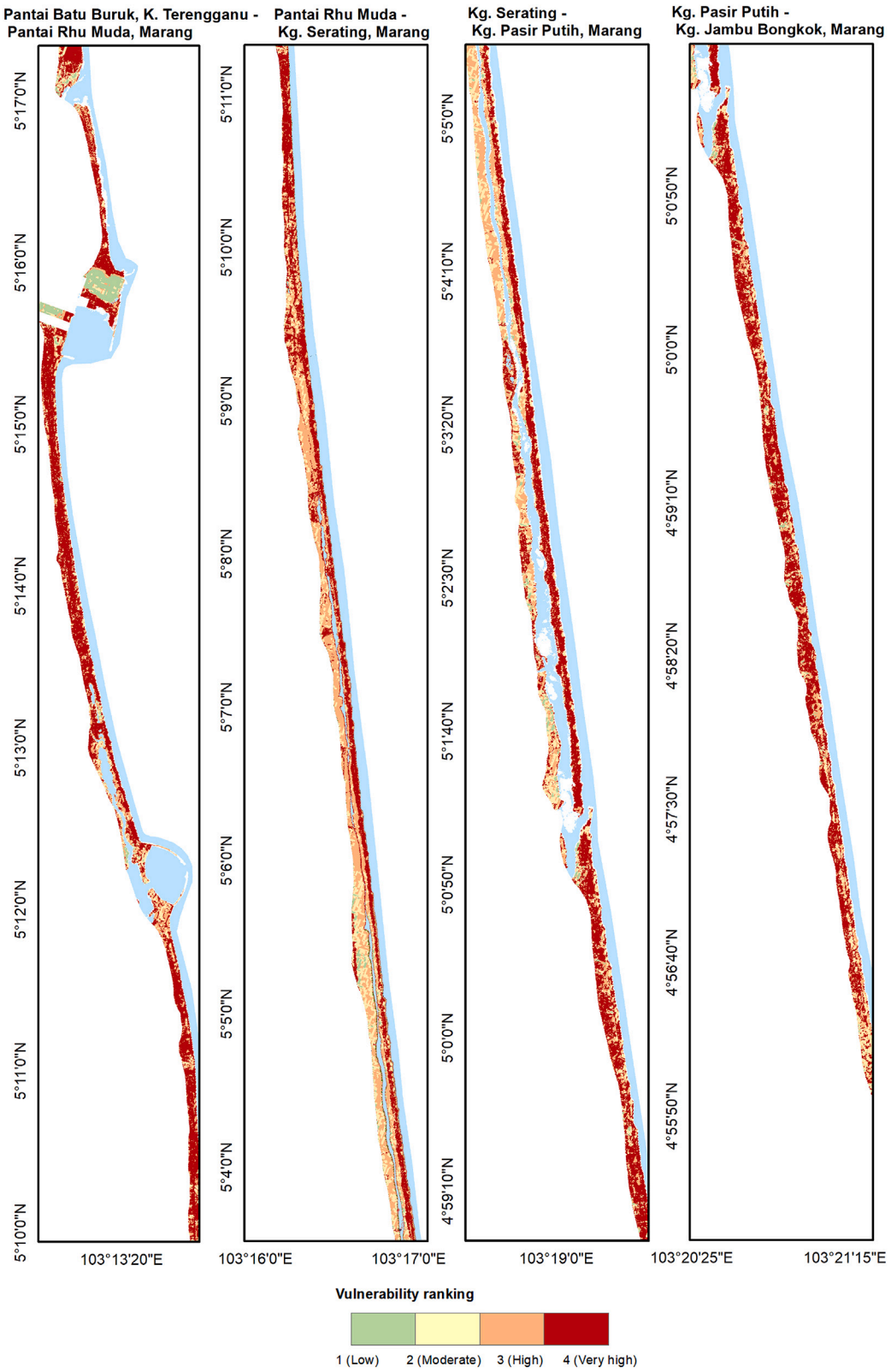

Figure 13. Final CVI from eight parameters from Kuala Terengganu to Marang

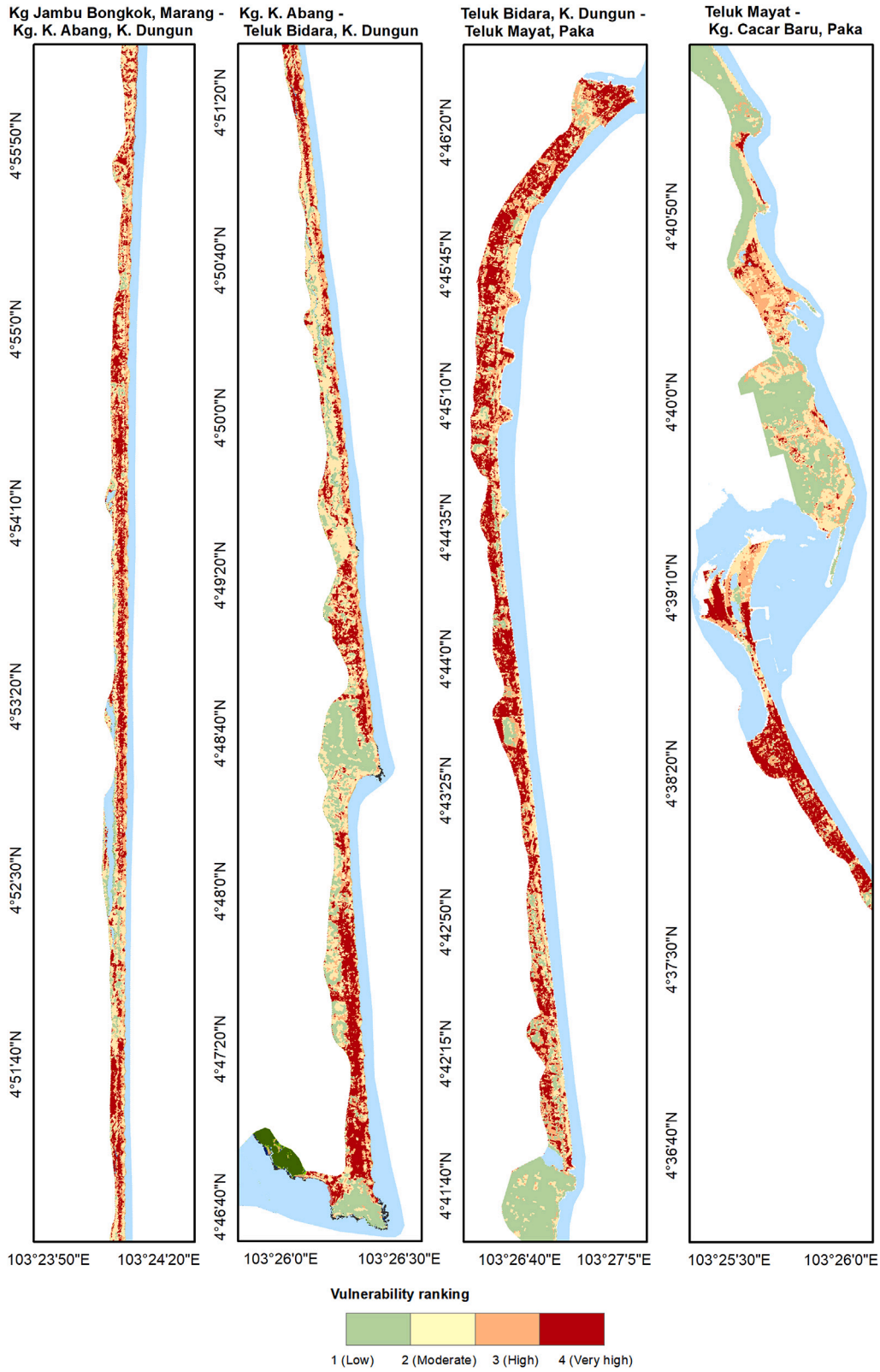

Figure 14. Final CVI from eight parameters classification from Marang to Paka

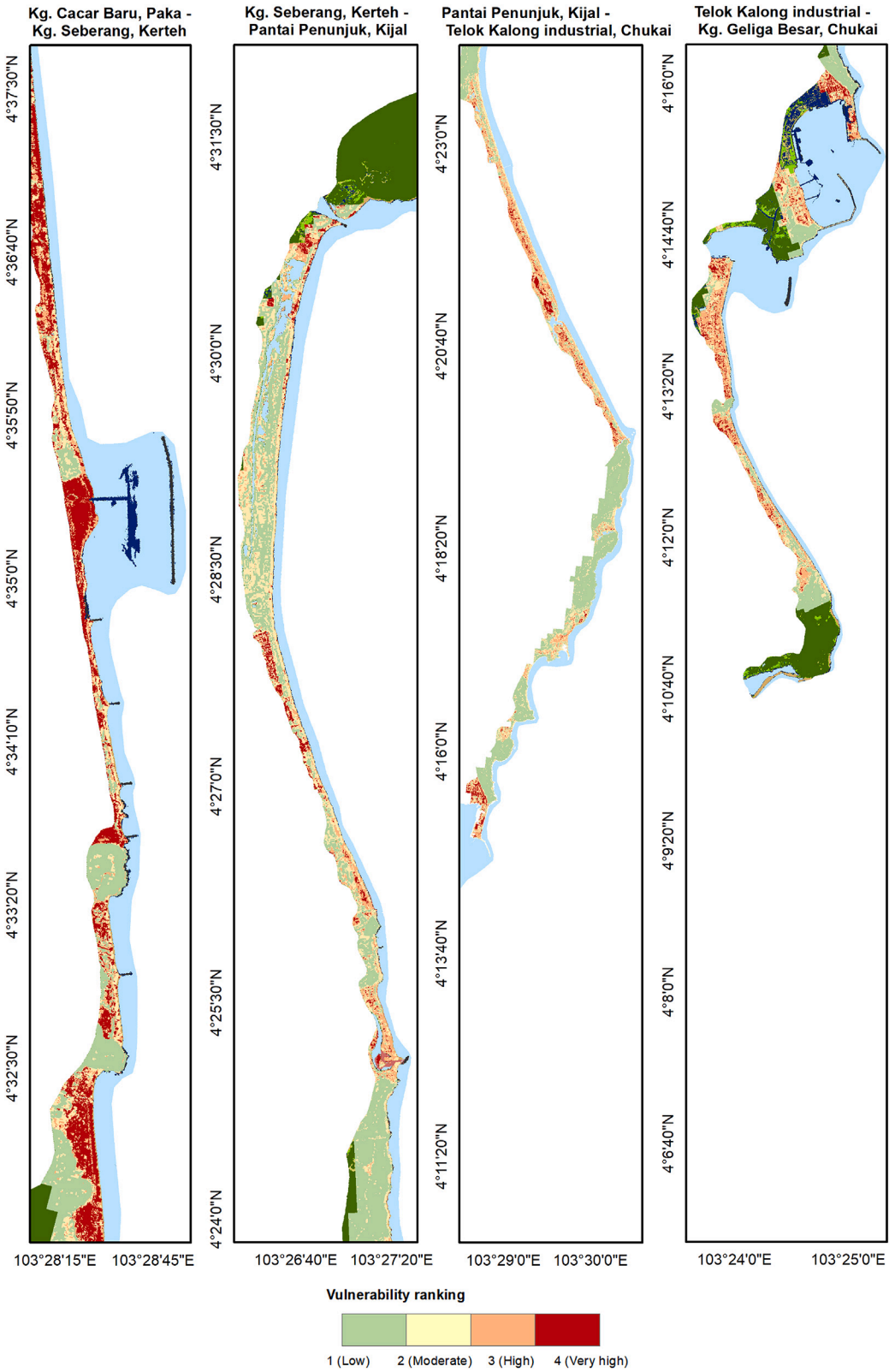

Figure 15. Final CVI from eight parameters from Paka to Chukai

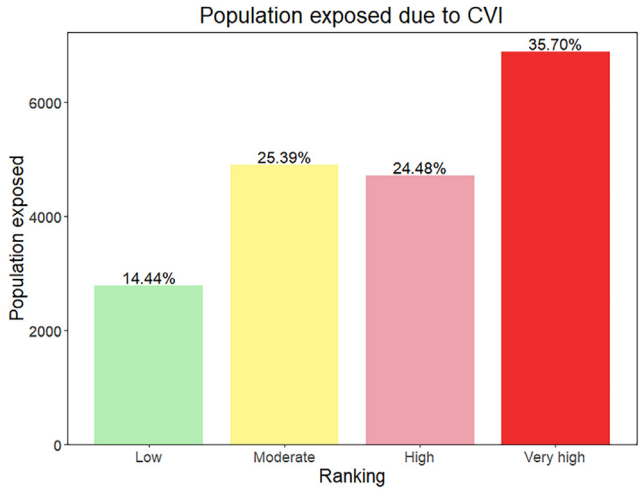

Figure 16. Terengganu population exposed according to CVI

The primary purpose of this research is to employ space-based physical variables as a viable tool for vulnerability assessment. Given the growing concern about the risk of coastal erosion, which is exacerbated by rising sea levels and climate change, it is imperative to conduct a comprehensive inspection on a broader scale. State-of-the-art space geodetic techniques are now conceivable, and as such, this study has assessed CVI from a range of satellites. Each physical variable utilized had been optimized, and following the evaluation, each parameter had shown encouraging results to be adapted to CVI. Analysis of the CVI with control ground also reveals promising outcomes. Estimating CVI from space-based measurements, however, faced several limitations. One of the main limitations when estimating CVI from space-based measurements is the difficulty in standardizing the duration of each variable. This task seems to be unrealistic due to different data collection durations of each sensor. Several parameters necessary to calculate the CVI in Terengganu coasts were also overlooked due to constraints in available techniques for their computation. Given that the coasts of Terengganu are characterized by beach slopes that provide protection during severe storms,[20] it is necessary to enhance research efforts in space-based methods for measuring beach dunes. Furthermore, the scarcity of large-scale data poses significant challenge, considering the associated costs of acquisition. Nonetheless, these limitations open up opportunities for future research.

All in all, the long-term goal of vulnerability assessment is to estimate coastal development to a certain degree of accuracy, which will be valuable for sustainable management in Malaysian coasts. Many studies on vulnerabilities have difficulty devising accurate and detailed approaches for risk resolution and identifying reliable mitigation strategies, particularly at the mesoscale. Space geodetic techniques offer many advantages, making them an alternative to conventional techniques while assisting in a practical coastal management framework. The information in this study is critical to attaining immediate and long-term goals of coastal management activities. As the studies on coastal vulnerability advances, the systems involved must also be analyzed progressively and extensively.

STAR★METHODS

Detailed methods are provided in the online version of this paper and include the following:

- KEY RESOURCES TABLE
- RESOURCE AVAILABILITY
  - Lead contact
  - Materials availability
  - Data and code availability
- METHOD DETAILS
  - Study area
  - Physical variables
- QUANTIFICATION AND STATISTICAL ANALYSIS
  - Analytical hierarchy process for CVI computation
  - Spatio-temporal analysis

ACKNOWLEDGMENTS

The authors would like to express gratitude to Universiti Teknologi Malaysia (UTM) for funding this research under the Professional Development Research University (PDRU), Vote Number Q.J130000.21A2.06E86 and UTM Fundamental Research (UTMFR), Vote Number Q.J130000.3852.22H75.

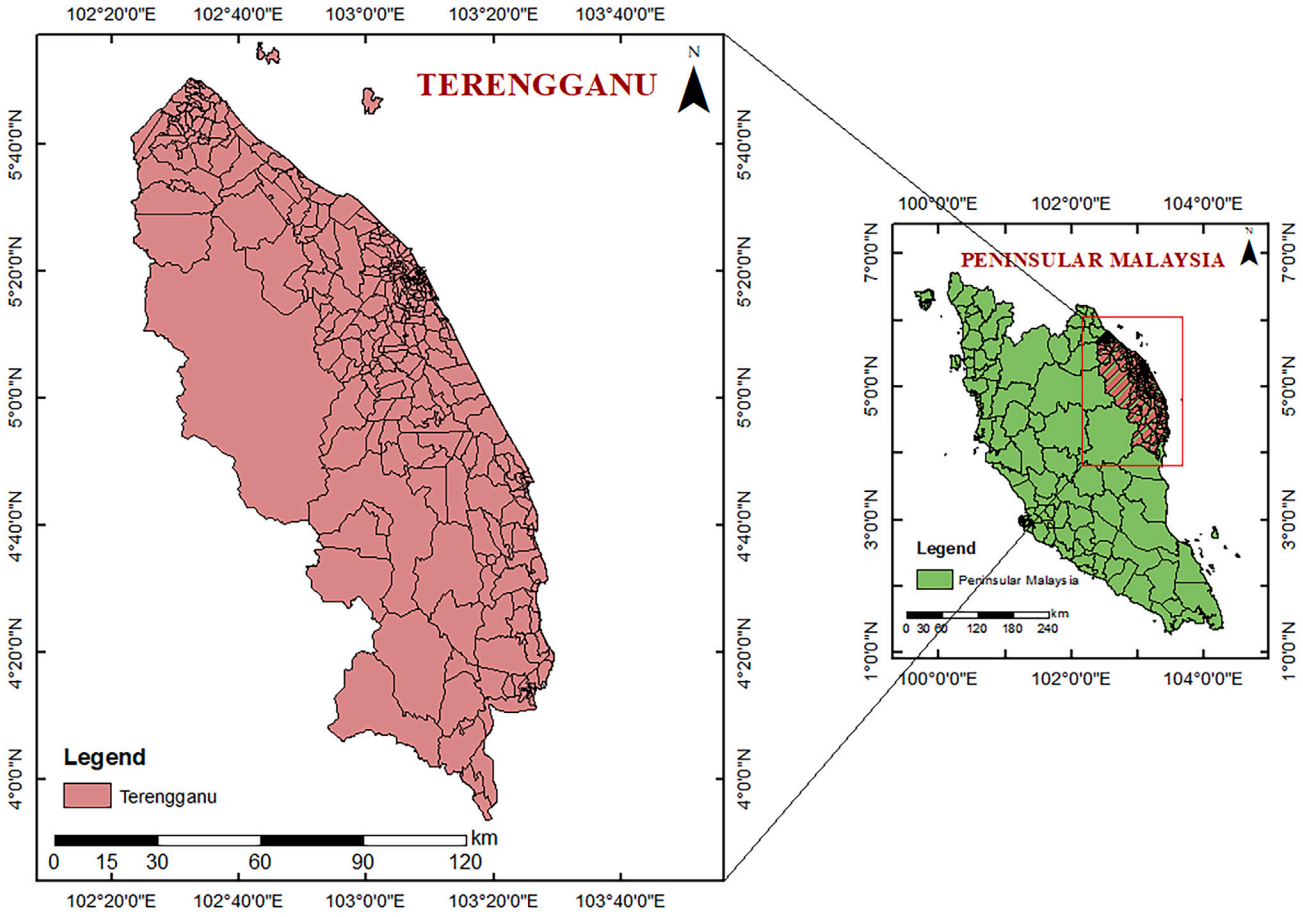

Figure 17. The region of Terengganu over Peninsular Malaysia

AUTHOR CONTRIBUTIONS

Conceptualization, A.I.A.H. and A.H.M.D.; methodology, A.I.A.H., M.H.H., and N.A.Z.; investigation, A.I.A.H., A.H.M.D., M.H.H., and N.A.Z., writing – original draft, A.I.A.H., writing – review and editing, A.I.A.H. and A.H.M.D; software, A.I.A.H., M.H.H., and N.A.Z.; validation, A.I.A.H.; frmal analysis, A.I.A.H.; supervision, A.H.M.D., N.Y., and N.M.A.; funding acquisition, A.H.M.D.; resources, A.H.M.D.

DECLARATION OF INTERESTS

The authors declare no competing interests.

Received: December 31, 2023
Revised: March 26, 2024
Accepted: May 20, 2024
Published: May 23, 2024

REFERENCES

1. Ramieri, E., Hartley, A.J., Barbanti, A., Santos, F.D., Gomes, A., Hilden, M., Laihonen, P., Marinova, N., and Santini, M. (2011). Methods for assessing coastal vulnerability to climate change. European Topic Centre on Climate Change Impacts, Vulnerability and Adaptation (ETC CCA), 1–93. https://www.cmcc.it/projects/etccca-european-topic-centre-on-climate-change-impacts-vulnerability-and-adaptation-2019-2021.

2. Rodrigues-Filho, J.L., Macêdo, R.L., Sarmento, H., Pimenta, V.R.A., Alonso, C., Teixeira, C.R., Pagliosa, P.R., Netto, S.A., Santos, N.C.L., Daura-Jorge, F.G., et al. (2023). From Ecological Functions to Ecosystem Services: Linking Coastal Lagoons Biodiversity with Human Well-Being (Springer International Publishing). https://doi.org/10.1007/s10750-023-05171-0.

3. Oppenheimer, M., Glavovic, B.C., Hinkel, J., van de Wal, R., Magnan, A.K., Abd-Elgawad, A., Cai, R., Cifuentes-Jara, M., DeConto, R.M., Ghosh, T., et al. (2019). Sea Level Rise and Implications for Low-Lying Islands, Coasts and Communities. In IPCC Special Report on the Ocean and Cryosphere in a Changing Climate, H.-O. Pörtner, D.C. Roberts, V. Masson-Delmotte, P. Zhai, M. Tignor, E. Poloczanska, K. Mintenbeck, A.

Alegría, M. Nicolai, and A. Okem, et al., eds. (Cambridge University Press), pp. 321–445. https://doi.org/10.1017/9781009157964.006.

4. Smit, B., and Wandel, J. (2006). Adaptation, adaptive capacity and vulnerability. Glob. Environ. Change *16*, 282–292. https://doi.org/10.1016/j.gloenvcha.2006.03.008.
5. Šimac, Z., Lončar, N., and Faivre, S. (2023). Overview of Coastal Vulnerability Indices with Reference to Physical Characteristics of the Croatian Coast of Istria. Hydrology *10*, 14. https://doi.org/10.3390/hydrology10010014.
6. Gornitz, V. (1990). Vulnerability of the East Coast, U.S.A. to Future Sea Level Rise. J. Coast Res. 201–237. Special issue no. 9. Proceedings of the Skagen Symposium (2-5 September 1990).
7. Thieler, E.R., and Hammar-Klose, E.S. (1999). National assessment of coastal vulnerability to future sea level rise: Preliminary results for the U.S. Atlantic Coast. U.S Geological Survey, Open File Report, 99–593. https://doi.org/10.3133/ofr00178.
8. Pantusa, D., D'Alessandro, F., Riefolo, L., Principato, F., and Tomasicchio, G. (2018). Application of a Coastal Vulnerability Index. A Case Study along the Apulian Coastline, Italy. Water *10*, 1218. https://doi.org/10.3390/w10091218.
9. Almaliki, A.H., Zerouali, B., Santos, C.A.G., Almaliki, A.A., Silva, R.M.d., Ghoneim, S.S.M., and Ali, E. (2023). Assessing coastal vulnerability and land use to sea level rise in Jeddah province, Kingdom of Saudi Arabia. Heliyon *9*, e18508. https://doi.org/10.1016/j.heliyon.2023.e18508.
10. Gill, J.A., Anwar, A.M., and Omar, K.S. (2014). Towards the implementation of continuous coastal vulnerability index in Malaysia: A review. J. Teknol. *71*, 1–10. https://doi.org/10.11113/jt.v71.3819.
11. Nassar, K., Mahmod, W.E., Fath, H., Masria, A., Nadaoka, K., and Negm, A. (2018). Shoreline change detection using DSAS technique: Case of North Sinai coast, Egypt. Mar. Georesour. Geotechnol. *37*, 81–95. https://doi.org/10.1080/1064119X.2018.1448912.
12. Quang, D.N., Ngan, V.H., Tam, H.S., Viet, N.T., Tinh, N.X., and Tanaka, H. (2021). Long-Term Shoreline Evolution Using DSAS Technique: A Case Study of Quang Nam Province, Vietnam. https://doi.org/10.3390/jmse9101124.
13. Hamden, M.H., Din, A.H.M., Alihan, N.S.A., Pa'Suya, M.F., Wijaya, D.D., and Che Cob, A.S. (2023). Accuracy assessment of quasi-seamless hydrographic separation models in Malaysian waters. Front. Earth Sci. *11*, 1110181. https://doi.org/10.3389/feart.2023.1110181.
14. Zulkifli, N.A. (2022). Vertical Land Motion Estimation Derived from Space-Based Geodetic Techniques. Ph.D, Thesis (Universiti Teknologi Malaysia).
15. Rashidi, A.H.M., Jamal, M.H., Hassan, M.Z., Sendek, S.S.M., Sopie, S.L.M., and Hamid, M.R.A. (2021). Coastal structures as beach erosion control and sea level rise adaptation in malaysia: A review. Water *13*, 1–34. https://doi.org/10.3390/w13131741.
16. Mahmud, M.R., Hashim, M., and Reba, M.N.M. (2017). How effective is the new generation of GPM satellite precipitation in characterizing the rainfall variability over Malaysia? Asia Pac. J. Atmos. Sci. *53*, 375–384. https://doi.org/10.1007/s13143-017-0042-3.
17. Sekovski, I., Del Río, L., and Armaroli, C. (2020). Development of a coastal vulnerability index using analytical hierarchy process and application to Ravenna province (Italy). Ocean Coast Manag. *183*, 104982. https://doi.org/10.1016/j.ocecoaman.2019.104982.
18. Roseli, N.H., and Akhir, M.F. (2014). Variations of Southern South China Sea Characteristics near Pahang. Sains Malays. *43*, 1389–1396.
19. Ariffin, E.H., Sedrati, M., Akhir, M.F., Daud, N.R., Yaacob, R., and Husain, M.L. (2018). Beach morphodynamics and evolution of monsoon-dominated coasts in Kuala Terengganu, Malaysia: Perspectives for integrated management. Ocean Coast Manag. *163*, 498–514. https://doi.org/10.1016/j.ocecoaman.2018.07.013.
20. D'Alessandro, F., and Tomasicchio, G.R. (2016). Wave–dune interaction and beach resilience in large-scale physical model tests. Coast. Eng. *116*, 15–25. https://doi.org/10.1016/j.coastaleng.2016.06.002.
21. Ramli, N., Majid, H.A.M.A., Nawawi, W.N.W., Ishak, F.A.C., and Maarof, S. (2022). The Antecedents of Household Acceptance on Food Waste Innovation Products in Terengganu. In Proceedings (MDPI), p. 75. https://doi.org/10.3390/proceedings2022082075.
22. Garba, N.N., Ramli, A.T., Saleh, M.A., Sanusi, M.S., and Gabdo, H.T. (2014). Terrestrial gamma radiation dose rates and radiological mapping of Terengganu state, Malaysia. J. Radioanal. Nucl. Chem. *303*, 1785–1792. https://doi.org/10.1007/s10967-014-3818-2.
23. Ariffin, E.H., Sedrati, M., Daud, N.R., Mathew, M.J., Akhir, M.F., Awang, N.A., Yaacob, R., Siddiqui, N.A., and Husain, M.L. (2019). In Chapter 5 - Shoreline Evolution Under the Influence of Oceanographic and Monsoon Dynamics: The Case of Terengganu, Malaysia, M. Ramkumar, R.A. James, D. Menier, and K. Kumaraswamy, eds. (Elsevier), pp. 113–130. https://doi.org/10.1016/B978-0-12-814350-6.00005-7.
24. Dong, W.S., Ariffin, E.H., Saengsupavanich, C., Mohd Rashid, M.A., Mohd Shukri, M.H., Ramli, M.Z., Miskon, M.F., Jeofry, M.H., Yunus, K., Ghazali, N.H.M., and Md Noh, M.N. (2023). Adaptation of coastal defence structure as a mechanism to alleviate coastal erosion in monsoon dominated coast of Peninsular Malaysia. J. Environ. Manage. *333*, 117391. https://doi.org/10.1016/j.jenvman.2023.117391.
25. Gonçalves, J., Pôças, I., Marcos, B., Mücher, C.A., and Honrado, J.P. (2019). SegOptim—A new R package for optimizing object-based image analyses of high-spatial resolution remotely-sensed data. Int. J. Appl. Earth Obs. Geoinf. *76*, 218–230. https://doi.org/10.1016/j.jag.2018.11.011.
26. Kılar, H. (2023). Shoreline change assessment using DSAS technique: A case study on the coast of Meriç Delta (NW Türkiye). Reg. Stud. Mar. Sci. *57*, 102737. https://doi.org/10.1016/j.rsma.2022.102737.
27. Rahman, M.F.A., Din, A.H.M., Hamid, A.I.A., Alihan, N.S.A., Yazid, N.M., Ansar, A.M.H., Pa'suya, M.F., Yamen, S.N.M., Khalid, N.F., and Junid, M.A.H. (2022). Accuracy assessment of open-source global digital elevation models (GDEMs) with global navigation satellite system (GNSS) levelling. IOP Conf. Ser. Earth Environ. Sci. *1064*, 012018. https://doi.org/10.1088/1755-1315/1064/1/012018.
28. Barata, M.B., Din, A.H.M., and Omar, A.H. (2019). In Wave Height Climatology Assessment from Multi-mission Satellite Altimeter for Renewable Energy BT - GCEC 2017, B. Pradhan, ed. (Springer Singapore), pp. 875–890.
29. Fok, H. (2012). Ocean Tides Modeling Using Satellite Altimetry. DPhil. Thesis (Ohio State University).
30. Byun, D.-S., and Hart, D. (2019). On Robust Multi-Year Tidal Prediction Using T_TIDE. Ocean Sci. J. *54*, 657–671. https://doi.org/10.1007/s12601-019-0036-4.
31. Din, A.H.M., Zulkifli, N.A., Hamden, M.H., and Aris, W.A.W. (2019). Sea level trend over Malaysian seas from multi-mission satellite altimetry and vertical land motion corrected tidal data. Adv. Space Res. *63*, 3452–3472. https://doi.org/10.1016/j.asr.2019.02.022.
32. Din, A.H.M., Nadzri, M., Reba, M.N.M., Omar, K., Pa'suya, M.F., and Ses, S. (2015). Sea level rise quantification using multi-mission satellite altimeter over Malaysian seas. In The 36th Asian Conference on Remote Sensing (ACRS 2015).
33. Hamid, A.I.A., Din, A.H.M., Abdullah, N.M., Yusof, N., Hamid, M.R.A., and Shah, A.M. (2021). Exploring space geodetic technology for physical coastal vulnerability index and management strategies: A review. Ocean Coast Manag. *214*, 105916. https://doi.org/10.1016/j.ocecoaman.2021.105916.
34. Jamaludin, S., Zin, W., Deni, S., and Jemain, A. (2010). Trends in Peninsular Malaysia Rainfall Data During the Southwest Monsoon and Northeast Monsoon Seasons: 1975-2004. Sains Malays. *39*, 533–542.
35. Ariffin, E.H., Sedrati, M., Akhir, M.F., Yaacob, R., and Husain, M.L. (2016). Open sandy beach morphology and morphodynamic as response to seasonal monsoon in Kuala Terengganu, Malaysia. J. Coast Res. *75*, 1032–1036. https://doi.org/10.2112/SI75-207.1.
36. Saaty, T.L. (1988). The Analytical Hierarchy Processes, 2nd edition (McGraw-Hill).
37. Duriyapong, F., and Nakhapakorn, K. (2011). Coastal vulnerability assessment: A case study of Samut Sakhon coastal zone. Songklanakarin J. Sci. Technol. *33*, 469–476.
38. Hammar-Klose, E.S., and Thieler, E.R. (2001). Coastal vulnerability to sea-level rise: a preliminary database for the U.S. Atlantic, Pacific, and Gulf of Mexico coasts. https://doi.org/10.3133/ds68.
39. Pendleton, B.E.A., Barras, J.A., Williams, S.J., Twichell, D.C., and Survey, U.S.G. (2010). Coastal Vulnerability Assessment of the Northern Gulf of Mexico to Sea-Level Rise and Coastal Change (USGS Publ). https://doi.org/10.3133/ofr20101146.

STAR★METHODS

KEY RESOURCES TABLE

REAGENT or RESOURCE	SOURCE	IDENTIFIER
Deposited data		
Landsat	NASA	https://developers.google.com/earth-engine/datasets/catalog/landsat
IMERG	GES DISC Distributed Active Archive Center	https://giovanni.gsfc.nasa.gov/giovanni/
TanDEM-X	EOC Geoservice	https://download.geoservice.dlr.de/TDM90/
Software and algorithms		
SegOptim package	Gonçalves et al.	https://github.com/joaofgoncalves/SegOptim
Google Earth Engine	Google	https://earthengine.google.com/
DSAS	United States Geological Survey (USGS)	https://www.usgs.gov/centers/whcmsc/science/digital-shoreline-analysis-system-dsas
Other		
RADS server in Universiti Teknologi Malaysia	Department of Earth Observation and Space Systems, TU Delft	http://rads.tudelft.nl/rads/rads.shtml

RESOURCE AVAILABILITY

Lead contact

Further information and requests for resources should be directed to and will be fulfilled by the lead contact, Dr Amalina Izzati Abdul Hamid (amalina.izzati@utm.my).

Materials availability

SPOT-6 satellite data utilised in this study are acquired from a private company, whereas the freely accessible Landsat data, are extracted using Google Earth Engine. Although TanDEM-X data at 30m and 90 m resolutions are freely available through website, TanDEM-X with resolution of 12m are obtained through personal contact with the Geoservice of European Comission. Significant wave height, SSH and SLA are extracted from the RADS server while IMERG data can be accessed publicly through Giovanni website.

Data and code availability

- All vital data relevant to the processing and analysis of coastal vulnerability assessment are mostly from public repositories, with only a few exceptions of granted repositories that accessible exclusively at the university or purchased through private company.
- All codes used for satellite data processing are written by the authors except those explicitly noted otherwise. These codes can be considerably shared by the lead contact upon request.
- Any additional information required to reanalyse the data reported in this paper is available from the lead contact upon request.

METHOD DETAILS

Study area

The area of the study is located along the coast of the Terengganu region in Peninsular Malaysia, as shown in Figure 17. Due to its strategic location facing the South China Sea, the region serves as a hub of marine tourism, with a population of around one million.[21] Strong coastal currents from the South China Sea transport sand to the Terengganu coast, resulting in sand covering about 90% of the coastal area, with weathered granitic sediment deposits predominating.[22] The South China Sea, an open sea, is a prospective area that exhibits an extensive supply of satellite data due to its location, which is also critical to this study. Terengganu coastline stretches for approximately 245 km, commencing from Kuala Besut in the north and ending at Kuala Kemaman. Several critical issues on why Terengganu has been selected as a study area are addressed, with one notable aspect being its proneness to erosion.[23] The majority of Terengganu's beaches consist of both natural and man-made beach dunes, serving as protective barriers over sandy coastlines against high waves and water levels during severe storms. However, the monsoonal regime in this region, particularly during the northeast monsoon,[24] combined with various topographic conditions, has led to the loss of many parts of the beaches in Terengganu, disrupting the natural equilibrium of sediment balance

and the longshore sediment drift circulation. The impact of the monsoon on Terengganu coastal erosion has also been investigated by incorporating the rainfall variable into the CVI.

Physical variables

Other than the six frequently used physical variables associated with rising sea related to coastal changes, which are: 1) geomorphology; 2) shoreline erosion/accretion rates (m/yr); 3) coastal slope (percent); 4) significant wave height (m); 5) tidal range (m) and 6) rate of sea level (mm/yr), this study incorporates additional physical variables of land subsidence/uplift (mm/yr) and rainfall intensity (mm/hour), as listed in see Table below.

Physical variables used for CVI assessment

Parameter	Sensor	Duration
Sea level rate rate	Multi-mission of satellite altimeters	1993-2019
Tidal range		
Significant wave height		
Geomorphology	SPOT	2019
Shoreline erosion/accretion	SPOT and Landsat	1996, 2002, 2013 and 2019
Coastal slope	TanDEM-X	2014
Land subsidence/uplift	GNSS, GRACE and tide gauge	1999-2017
Rainfall intensity	GPM and TRMM (IMERG)	2000-2019

Since this paper emphasises the use of space-geodetic and optical imaging techniques for deriving coastal variables, this section describes the necessary steps to be taken in the process. Subsequently, a proportion of the risk rating was assigned to each variable prior to the computation of CVI. The WGS84 coordinate system was mainly used for the geodetic datum realisation of this study. The approaches to derive each physical variable were as follows:

Geomorphology

Considering that the CVI study presented in this paper heavily relied on space-based techniques to assess variables, one of which was evaluating the large-scale geomorphology of the Terengganu coastal area using optical imagery, it was imperative to classify the imagery correctly. SPOT 6 of the multi-spectral image from the 2018-2019 epoch and 1.5 m spatial resolution was used for this purpose. Two types of classification were employed: standard supervised classification and optimised segmentation of object-based image analysis (OBIA) from the SegOptim package in R. Training samples were collected in the form of polygons representing the region of interests (ROI), and identical training samples were used for both classification processes. The SegOptim package, developed by Gonçalves et al.,[25] was utilised to classify complex areas to overcome ambiguities in supervised classification. The advantage of this package lies in its application of genetic algorithms to optimise multiple image segmentation parameters. However, SegOptim relies on third-party software to perform segmentation due to the inherent complexity of segmentation algorithms and their implementations. The segmentation algorithm used for this assessment was from Orfeo Toolbox of large-scale mean-shift algorithm, which the developer recommends as it can comprehend big satellite data to execute accurate segmentation. Once the optimisation parameters in charge of regulating the initial population had converged, final segmentation and classification were executed within the package. Finally, the classified images from both classifications were merged through a 'blend' analysis in Geographic Information System (GIS) software.

Shoreline erosion or accretion

The working principle underlying shoreline erosion/accretion derivation is similar to geomorphology when optical satellite is used. Nevertheless, the classification of overall multi-spectral images is not as pivotal as the delineation between land and sea areas. SPOT 6 from the epoch 2018-2019 was used again to identify shoreline changes along the Terengganu coast, supplemented by additional satellites, namely historical SPOT 6 from the epoch 2013-2014, as well as Landsat imagery from the epochs of 1994-1996 and 2001-2002. All satellite imageries used to analyze shoreline erosion/accretion underwent normalised difference water index (NDWI) analysis,[26] which is recognized for highlighting open water features in satellite imagery, accentuating the delineation of water bodies. Landsat images were acquired through Google Earth Engine (GEE), a cloud-based platform that facilitates access to high-performance computing resources for geospatial data processing. In this study, the code was developed to emphasize cloud masking, acquisition, pre-processing, and NDWI analysis. It was also tailored to autonomously populate the study area with cloud-free images using numerous image combinations at varying epochs, thus enhancing practicality and time efficiency. Following that, the rate of shoreline erosion/accretion was calculated using the Digital Shoreline Analysis System (DSAS), a software extension within the GIS environment, where transects were automatically cast along the Terengganu shoreline based on the user-created baseline before performing the rate calculation.

Coastal slope

In this study, the coastal slope was derived from the landward beach elevation to the shoreline. Instead of using a bathymetry model, this approach was used to demonstrate the coastal area's condition. TanDEM-X, a publicly available digital elevation model (DEM), was used to derive coastal slope information owing to its high accuracy over Peninsular Malaysia.[27] Combining 12 m with 30 m was performed by mosaicking the DEM raster datasets to create a single raster. The extraction of the Terengganu coastal slope was carried out in the slope analysis within GIS software, determining the slope inclination as a percent rise, also known as the percent slope. Since a projected coordinate system is required to compute distance slope in metres, the geographical WGS84 was converted to the projected coordinate system of WGS84 UTM zone 48. Nevertheless, in order to perform spatio-temporal analysis of coastal slope with Global Navigation Satellite System (GNSS) levelling, orthometric heights (H) derived from TanDEM-X were computed relative to local reference coordinate to align with the local datum used during GNSS levelling and the local geoid height.

Significant wave height

Significant wave height is the average of the highest one-third proportion of waves in a spectrum. In contrast to the traditional buoy-based acquisition of wave height data, satellite altimeters can only measure significant wave height signals by analysing backscattered microwave pulses reflected at the sea surface.[28] This study employed 12 satellite altimeter missions to obtain significant wave height from 1993-2019, executed within the Radar Altimeter Database System (RADS). Developed by the Delft Institute for Earth-oriented Space Research (DEOS), RADS is a database system that integrates authenticated altimetry products which consistently maintained by the international scientific community. In the initial step of RADS processing, a shell script was created to define the geographical coordinates of the study area and incorporate essential parameters for retrieving significant wave height. The correction and bias removal were applied during the retrieval process. Significant wave heights obtained from the satellite altimeter were spatially gridded with a block size of 0.25° to cover extensive sea areas by using inverse distance weighted (IDW) interpolation before undergoing data filtering. The final step involves averaging the monthly significant wave heights retrieved from RADS over the study period.

Tidal range

Tidal signals over deep oceans have historically not been a significant concern, but contemporary scientists have explored the use of satellite altimeters to provide deep ocean tidal signals through tide modelling. Hamden et al.[13] predicted a tidal datum called UTM20 across Malaysian seas by combining coastal tide gauge data with satellite altimetry-derived sea surface heights (SSH) model. To predict tides from tidal analysis, continuous tidal data in short intervals between minutes and days is preferable for accurate tidal signal reading. While satellite altimeter proves valuable in providing continuous data, its temporal sampling rate of once a week to every 35 days due to its orbital design renders it impractical to provide tidal data at shorter intervals. Since tidal range demands an actual value with small temporal sampling, along-track satellite altimeter data are currently the best option for predicting the tide model from space. RADS was used to pre-process sea surface height (SSH) acquired from along-track altimeter data based on the optimal range and geophysical correction for the Malaysian region. Ocean tide correction was not applied in the RADS shell script to minimise the loss of tidal signal in altimeter-derived SSHs. SSH data from each altimeter mission were arranged in an orderly manner. In cases where redundant data existed at the end date, it was truncated to align with the commencement of the next altimeter mission.

Harmonic analysis was subsequently used to predict the tide model, excluding the ERS-class missions from the process due to their sun-synchronised orbit, which makes the prediction of solar tides and the semidiurnal S_2 signal implausible. However, given the temporal sampling limitations of satellite altimeters, it is crucial to address tidal aliasing. This issue can be solved by applying tidal aliasing information to harmonic analysis.[29] From harmonic analysis, the amplitudes and phases of 12 harmonic tidal constants were derived and these constants were then used to predict the along-track highest astronomical tide (HAT) and lowest astronomical tide (LAT) models. These models are based on tide predictions over the minimum duration of 19 years, as suggested by Byun et al.[30] Due to the inevitable degradation of altimeter footprints near the coast, the gridded HAT and LAT from the altimeter were truncated within 20 km from the coast to minimise the influence of altimetric noises. Afterward, the HAT and LAT above zero tide gauges, derived from the coastal tide gauge, were integrated with the altimetry HAT and LAT models using the Thin Plate Spline approach. The tidal range was subsequently computed from the vertical difference between HAT and LAT. It is worth noting that in this paper, the term "tidal range" is used instead of the traditional term "mean tidal range". This distinction arises because the tidal range in this study was derived from integrating two types of measurements as opposed to being traditionally derived from the average of continuous tide gauge data.

Sea level rate

To calculate sea level rate, altimetry sea level anomaly (SLA) data from satellite altimeters were retrieved through RADS. The process involved using the same 12 satellite altimeter missions that were used to retrieve significant wave height. The principle of obtaining sea level anomaly data from satellite altimeters is also similar to significant wave height. However, the sea level signal from the satellite altimeter is based on the round trip of short-wave microwave rays travelling from the satellite to the sea surface, with the main parameter of range, R, being derived.[31] Sea level data underwent crossover adjustment within the RADS framework, a RADS-only component of dual-crossover minimisation analysis to reckon errors and refine altimeter observations. Crossover minimisation is accomplished when the European Space Agency (ESA) -class satellites are adjusted to the National Aeronautics and Space Administration (NASA) -class satellite orbits, as the stability of NASA-class

satellite orbits surpasses the ESA-class satellite orbits. Following crossover adjustments, daily altimetry data were filtered and gridded to the SLA at predefined bin sizes using Gaussian weighting functions.[32] Distant weighting functions were applied to obtain meaningful values for grid points by assigning larger weights to points closer to the centre located between tracks. Daily SLAs were then aggregated into monthly average solutions. Eventually, the sea level rates over the Terengganu coast were estimated using the robust fitting method, a statistical method that deals with solution determination and outlier detection. This method uses the Iteratively Re-weighted Least Squares (IRLS) technique to fit the SLA time series to a linear function and then solve for trends in the function while identifying the SLA outliers.

Land subsidence or uplift rate

It is important to highlight that satellite altimeter provides absolute anomalies, whereas relative anomalies for sea level changes (including land motion) have been customarily used for CVI studies. This is because of topographical concerns, in which land subsidence or uplift data are the main indicators of flood risk assessment.[6,33] Therefore, it is necessary to include information on land motion to account for absolute anomalies identified by satellite altimeters. Zulkifli[14] outlined a methodology for calculating the rate of land subsidence/uplift by integrating land motion information from the Global Navigation Satellite System (GNSS), Gravity Recovery and Climate Experiment (GRACE), satellite altimeters and tide gauges. GNSS datasets from 53 IGS stations were employed as reference stations to connect 78 local CORS data to the global reference frame, which were post-processed in high-precision GNSS data processing software.

Concurrently, land motion information derived from GRACE satellites was quantified regarding terrestrial water storage (TWS) and groundwater storage (GWS). The resulting vertical displacements generated from both sets of information were used to calculate the land subsidence/uplift rate from GRACE. The conclusive rates from both measurements, computed from the time series of final GNSS coordinates and GRACE-derived vertical displacement, were determined using robust fitting. The calculation of land subsidence/uplift rate from satellite altimeter and tide gauge mainly involves manipulating the absolute and relative SLA from both measurements. The direct approach corrects tide gauge records from the influence of land motion and is limited to measuring coastal tide gauges at a single point. The double difference approach, on the other hand, is versatile, applicable anywhere, and involves determining the relative vertical motion between two land motion records rather than at a single tide gauge point. They underwent similar robust fitting analysis, followed by the direct and double difference approaches to estimate the final rate derived from satellite altimeters and tide gauges.[14] Ultimately, a least square collocation was applied to integrate the land subsidence/uplift rate derived from multiple sensors used in this study. Since the optimal inputs have been utilised to obtain the best rate, the estimated land subsidence/uplift rate was not subjected to spatio-temporal analysis.

Rainfall intensity

Northeast monsoon has predominantly influenced rainfall patterns in eastern Peninsular Malaysia, resulting in strong waves along the coast.[34] This condition erodes a substantial segment of the beach profile, though recovery is possible during the Southwest monsoon. Regardless, a study by Ariffin et al.[35] demonstrated that the developed beaches in Terengganu did not recover from the post-storm states. The strong current contributes significantly to erosion, particularly during seasons characterized by severe shoreline erosion, underscoring the importance of incorporating the rainfall intensity parameter into the CVI. IMERG common precipitation product blends precipitation data from the Global Precipitation Measurement (GPM) satellite constellation with early precipitation estimates from the now-defunct Tropical Rainfall Measuring Mission (TRMM) satellite. IMERG Final Precipitation L3 1-month V06, which was derived from the half-hour GPM estimates, was used for this study, providing the final estimate of daily cumulative precipitation. NASA recommends using the final run product since they incorporate month-to-month adjustments, which add up to the final run monthly satellite-gauge combination. IMERG's rainfall intensity data was obtained from the time-averaged map available in the Giovanni website (a web application hosted by the NASA Goddard Earth Science Data and Information Services Center (GES DISC) Distributed Active Archive Center (DISC), that offers an intuitive platform for visualizing, analysing, and accessing Earth science remote sensing data, mainly from satellites), which did not account for the short-term precipitation effect over one hour (as estimated by the Intensity-Duration-Frequency or IDF curve). Instead, the acquired intensity was calculated from the intensity of annual means, which was computed by dividing the total rainfall by the number of hours within the data's duration.

QUANTIFICATION AND STATISTICAL ANALYSIS

Analytical hierarchy process for CVI computation

Analytical Hierarchical Process (AHP) is extensively used in decision-making problems for its ability to prevent arbitrary weight allocation.[17,36] Hence, it was used in CVI assessment to determine the weight of each variable by consolidating the opinions of seven experts knowledgeable about the coastal process of the study area. This was achieved using a questionnaire of pairwise comparison analysis, encompassing feedback from policymakers to academicians. With a comparison matrix, a priority vector, which is essentially the matrix's eigenvector, was computed. Each variable was then assigned a weighted score reflecting its importance and relevance in the level of vulnerability of the coastal area to erosion. To ensure the consistency of the subjective perception and the accuracy of the comparing weights, two indicators, the consistency index (C.I.) and consistency ratio (C.R.), were initially calculated. Experts with C.I. values exceeding 0.1 threshold were excluded.[17] Consequently, the final weighted value of each physical variable was determined by multiplying the average weight of the successful experts' scores by the risk value, as shown in Equation 1 below:[37]

$$W_n = \sum_{i=1}^{n} f_i \,.\, w_i \qquad \text{(Equation 1)}$$

where W_n is the final weighted value and f_i is the vulnerability ranking of each variable of factor i, and w_i is the weight of each variable. The relative risk value was then allocated to each physical variable across uniformly sized pixel images, given the large spatial extent of the study area. This allocation reflects the magnitude of its potential impact on coastal changes. Finally, the CVI was calculated as the square root of the product of the ranked variables divided by the total number of variables.[38,39]

Spatio-temporal analysis

Spatio-temporal analysis is conducted to ensure the reliability of the input data of the CVI. Each principal variable is compared with its respective in-situ measurements. The variables are analysed in terms of mean bias (*MB*), root mean square error (*RMSE*), and Pearson's correlation of determination (*R*). For the geomorphology variable, a confusion matrix of overall accuracy (*OA*) as well as Cohen's *Kappa* coefficient is computed while the shoreline erosion variable is analysed based on the metrics derived from DSAS, specifically End Point Rate (*EPR*) and Linear Regression Rate (LRR). Coastal slope variable is assessed based on orthometric heights. In addition to metrics such as *MB*, *RMSE* and *R*, categorical indices of probability of detection (*POD*), false alarm ratio (*FAR*), and crucial success index (*CSI*) are used to represent the occurrence of precipitation events. A list of the metrics used in the spatio-temporal analysis is given below.

Comparison is carried out to determine whether a CVI based on six or eight parameters provided a more accurate vulnerability assessment. A suite of metrics was employed: *OA*, Kappa coefficient, Receiver Operating Characteristic (ROC) curve, and Area Under the Curve (*AUC*). These metrics comprehensively assessed the agreement between the predicted vulnerability categories and the ground truth data, allowing for an objective evaluation of the optimal number of CVI parameters.

Metrics used in the spatio-temporal analysis

Acronym	Metrics Name	Formula	Unit
MB	Mean Bias	$MB = \frac{1}{n}\sum_{i=1}^{n} Y_i - X_i$ where n denotes the number of observations, X_i represents the observed in-situ measurement whereas Y_i denotes the space-geodetic measurement of corresponding variables.	m or mm
RMSE	Root Mean Square	$RMSE = \sqrt{\frac{1}{n}\sum_{i=1}^{n}(Y_i - X_i)}$ where n denotes the number of observations, X_i represents the observed in-situ measurement whereas Y_i denotes the space-geodetic measurement of corresponding variables.	m or mm
R	Pearson's Correlation of Determination	$R = \frac{\sum_{i=1}^{n}(X_i - \overline{X})(Y_i - \overline{Y})}{\sqrt{\sum_{i=1}^{n}(X_i - \overline{X})^2}\sqrt{\sum_{i=1}^{n}(Y_i - \overline{Y})^2}}$ where n denotes the number of observations, X_i and $\overline{X}$ represent the observed in-situ measurement and mean in-situ measurement, respectively, whereas Y_i and $\overline{Y}$ denote the space-geodetic measurement and mean of space-geodetic measurement, respectively, of corresponding variables.	-
OA	Overall Accuracy	$OA = \frac{\sum_{i=1}^{q} n_{ii}}{n} \times 100\%$ where q is the number of classes where n is the considered pixel total number, n_{ii} is the diagonal elements of the confusion matrix, n_{i+} represents the marginal sum of the rows in the confusion matrix, and n_{+i} represents the marginal sum of the columns in the confusion matrix.	%

(*Continued on next page*)

Continued

Acronym	Metrics Name	Formula	Unit
Producer's accuracy		$Producer's\ accuracy = \frac{n_{ii}}{n_{i+}} \times 100\%$ where q is the number of classes where n is the considered pixel total number, n_{ii} is the diagonal elements of the confusion matrix, n_{i+} represents the marginal sum of the rows in the confusion matrix, and n_{+i} represents the marginal sum of the columns in the confusion matrix.	%
User's accuracy		$User's\ accuracy = \frac{n_{ii}}{n_{+i}} \times 100\%$ where q is the number of classes where n is the considered pixel total number, n_{ii} is the diagonal elements of the confusion matrix, n_{i+} represents the marginal sum of the rows in the confusion matrix, and n_{+i} represents the marginal sum of the columns in the confusion matrix.	%
Kappa	Cohen's Kappa coefficient	$Kappa = \frac{n\sum_{i=1}^{q} n_{ii} - \sum_{i=1}^{q} n_{i+}n_{+i}}{n^2 - \sum_{i=1}^{q} n_{i+}n_{i+}} \times 100\%$ where q is the number of classes where n is the considered pixel total number, n_{ii} is the diagonal elements of the confusion matrix, n_{i+} represents the marginal sum of the rows in the confusion matrix, and n_{+i} represents the marginal sum of the columns in the confusion matrix.	%
EPR	End Point Rate	$EPR = \frac{D_A - D_B}{Date\ A - Date\ B}$ where D_A and D_B is the distance of shoreline movement calculated from point A and B from baseline, divided by the changes between those two elapsed shorelines.	m/yr
LRR	Linear Regression Rate	$L = b + mx$ where L is a dependent variable that represents the shoreline's geographic position, x denotes independent variable of year, m and b are the slope and intercept, respectively, that representing the change in L resulting from a change in x per unit or LRR.	m/yr
H	Orthometric Height	$H_{TanDEM-X} = h_{TanDEM-X} - N_{MyGeoid}$ where $H_{TanDEM-X}$ represents the orthometric height of TanDEM-X, $h_{TanDEM-X}$ is the ellipsoidal height extracted from Global Mapper and $N_{MyGeoid}$ represents the local geoid height model.	m
POD	Probability of Detection	$POD = \frac{a}{a+c}$ where a is the number of correct occurences detected by IMERG when compared to rain gauge, b represents the occurences that are wrongly reported by IMERG, and c is the precipitation occurences missed by the IMERG but detected by rain gauge.	-

(*Continued on next page*)

Continued

Acronym	Metrics Name	Formula	Unit
FAR	False Alarm Ratio	$FAR = \frac{b}{a+b}$ where *a* is the number of correct occurences detected by IMERG when compared to rain gauge, *b* represents the occurences that are wrongly reported by IMERG, and *c* is the precipitation occurences missed by the IMERG but detected by rain gauge.	-
CSI	Crucial Success Index	$CSI = \frac{a}{a+b+c}$ where *a* is the number of correct occurences detected by IMERG when compared to rain gauge, *b* represents the occurences that are wrongly reported by IMERG, and *c* is the precipitation occurences missed by the IMERG but detected by rain gauge.	-
ROC	Receiver Operating Characteristic	$TPR = \frac{TP}{TP+FN}$ $FPR = \frac{FP}{FP+TN}$ where *TP* stands for true positive and *FN* for false negative. *FP* is false positive and *TN* is true negative. On the ROC curve, two axes of true positive rate (*TPR*) and false positive rate (*FPR*) are determined.	-
AUC	Area Under the Curve	$AUC = \int TPR\, d(FPR)$	-